Effect of Iron Redox Ratio on the Structures of Boroaluminosilicate Glasses

Manzila I. Tuheen, Wei Sun, Jincheng Du*
Department of Materials Science and Engineering, University of North Texas, Denton, Texas
(*corresponding author. Email: du@unt.edu)

Abstract

Iron oxide is commonly found in natural or industrial glass compositions and can exist as ferrous (Fe^{2+}) to ferric (Fe^{3+}) species, with their ratio depending on the redox reactions during the glass forming process. Iron redox ratio plays an important role on silicate glass structures and consequently various properties. This work aims to study the effect of iron oxide, and particularly the iron redox ratio, on the structures of borosilicate and boroaluminosilicate glasses using molecular dynamics (MD) simulations with newly developed iron potential parameters that are compatible with the borosilicate potentials. The results provide detailed cation coordination states of both iron species and the effect of redox ratio on boron coordination and other structural features. Particularly, competition for charge compensation modifier cations (such as Na^{+}) among the four-fold coordinated cations such as B^{3+}, Al^{3+} and $Fe^{3+}$are investigated by calculating the cation-cation pair distribution functions, bond angle distributions and coordination preferential ratios. The results show that the tri-valent ferric ions act as a glass former whereas the di-valent ferrous ions mainly play the role of glass modifier. The ferrous/ferric ratio (Fe^{2+}/Fe^{3+}) was found to affect the glass chemistry and hence glass properties by regulating the amount of four-coordinated boron. The results are compared with available experimental data to gain insights of the complex structures and charge compensation schemes of the glass system.

1. Introduction

Borosilicate and boroaluminosilicate glasses are of significant importance due to their wide applications in technology fields ranging from insulating and reinforcing glass fibers, thermal shock and chemical resistant glass containers, optical components, to soft tissue repair for biomedicine and media for immobilization of radioactive nuclear waste[1–7]. Due to the presence of multiple glass network formers such as boron oxide, silica and alumina along with their

interactions with one or more network modifiers, this causes complex interactions among the glass formers that lead to mixed former effect and give rise to peculiar structure-property relations of these glasses.[8,9] The structures of borosilicate and boroaluminosilicate glasses have been investigated by experimental techniques such as ^{11}B solid state nuclear magnetic resonance (NMR) and models based on these analyses provide insights on the structures of these glasses[10–12]. One of the most important structural features is boron N_4 value, which denotes the fraction of four-fold coordinated boron. Addition of modifiers such as Na_2O or CaO to borate or borosilicate glasses causes the conversion of three-fold coordinated boron ($B^{[3]}$) to four-fold coordinated boron ($B^{[4]}$), while further increment of the concentration of modifier the amount of four coordinated boron reaches a maximum.[13,14] With even further addition of the modifier, four coordinated boron reverts back to three coordinated ones. These changes were later found to be a function of the silica to boron oxide ratio (K) and these were described well in the Dell, Bray and Xiao (DBX) model based on ^{11}B NMR studies.[13,14] Furthermore, it was found that boron coordination also depends on the modifier cation field strength[12,15] and addition of other oxides such as alumina[16]. For iron oxide containing borosilicate glasses, however, there are difficulties to study boron coordination by using solid state NMR due to the paramagnetic nature of iron ions.[17] This makes other approaches such as molecular dynamics simulations a valuable tool in understanding the complex structures of these glasses.

Iron containing silicate minerals are commonly found on earth's mantle and iron is also one of the most abundant elements in magma[18] and the physio-chemistry of the silicate melts thus determines the magmatic and volcanic process[19]. Discussion of iron containing silicate melt is therefore also relevant in the field of geological processes and numerous researches have been established and ongoing in this sector[20–22]. In multi-component iron (~7 wt%) containing silicates such as stone wool fibers (SWF), iron plays an important role in the formation of nanocrystalline layer which provides this glassy material with high temperature stability[23]. Fe bearing silicate melts were studied in forms of alkaline iron silicate melts and binary systems of iron silicates [18,24,25]. While in terrestrial igneous rock the FeO present is found to be up to 15% whereas in nuclear waste is of up to 25% [20,26]. The glassy structure of such melt is often taken to be as representative although there should be some deviation in cation coordination, density and iron redox ratio. Synchrotron X-ray diffraction along with aerodynamic levitation method allows the

in-situ analysis of melt structure. Recently, such methods were coupled with MD simulations to better understand the Fe bearing silicate melts [27].

Iron oxide is commonly found in silicate glasses either as an additive or from impurities of raw materials. Iron can exist in di- (Fe^{2+}) and tri-valent oxidation states (Fe^{3+}), known as ferric or ferrous ion respectively. Previous studies suggest that these two types of iron have different roles in the glass structure: the di-valent ferrous ions behave as a network modifier whereas the tri-valent ferric ions are often found to play the role of a network former[28–31]. It becomes even more complicated by the presence of multiple coordination states of both of these ions. In a system of boroaluminosilicate glasses, the interaction of Fe^{3+} ion along with other glass network formers such as Si, B, Al needs to be understood. Also, the role of Fe^{2+} as a network modifier and how different network formers compete for modifier cations for charge compensation is still unclear. As the ratio of ferrous and ferric iron changes with the melting environment, the redox ratio of the glass can play an important role on the structures and properties of these glasses.[32,33]

Understanding how iron oxide affects the structure and properties of borosilicate melt and glass is particularly important in the immobilization of nuclear waste through vitrification.[34]Immobilizing radioactive nuclear wastes in a borosilicate glass matrix, a process also known as vitrification, is a well-accepted way among the international community[35], due to the high chemical durability of the waste glasses and the relatively low melting temperature of glass processing[36,37].Iron is one of the most common transition elements found in borosilicate nuclear waste glasses[38,39]. Iron oxide greatly affects silicate melt and glass properties such as viscosity, crystallization behaviors, chemical durability and surface properties[40,41].The composition, temperature, pressure, and oxygen fugacity can all significantly affect the iron redox ratio, which in turn affect various properties of the glass waste forms[28].To understand the property changes of these waste glasses, it is important to understand the effect of iron redox ratio on the short and medium range structures.

A number of experimental characterization methods have been used to probe the structures of iron containing glasses. It has been shown by extended X-ray absorption fine structure (EXAFS) and X-ray absorption near edge structure (XANES) investigations that ferric iron mainly exist as four-fold coordination[42–45], while spectroscopic structural evidence shows the existence of five- and six-fold coordination[42,46]. The dominant four-fold coordination of ferric species make it easier to enter the silicate network hence play the role of a glass former[28,33,47]. The coordination number

of ferrous iron, on the other hand, is more debated. Earlier studies suggest that Fe^{2+} has a coordination number of six in silicate glasses and acts as network modifier.[28,32,48] Later studies show that the ferrous iron coordination in silicate glasses and melts can range from four to six.[30,49,50] In alkaline-earth alumina-silicate glasses, Fe^{2+} has been reported to show five- or six-fold coordination.[28] Cochain et al. reported that the coordination number of Fe^{2+} is mostly five and six in borosilicate glasses.[33]

Classical molecular dynamics has been proved to be an efficient way to provide systematic studies on short- and medium-range structures in multi-oxide glasses[34,51–54]. The existence of two oxidation states of iron and composition dependence of coordination change of boron makes simulations of iron oxide containing borosilicate glass a great challenge. Recently, Deng and Du[55] has reported a sets of partial charge pairwise potential for borosilicate glasses that is compatible for a large number of cations. The composition dependent boron parameter makes the potential capable of correctly reproduce boron coordination change with compositions in wide composition ranges and different glass systems. The purpose of this work is to introduce compatible potential parameters for ferric and ferrous ions and to use these potentials to investigate the structural roles of Fe^{3+} and Fe^{2+} in borosilicate glasses by using molecular dynamics simulations. The glass compositions were chosen from simplified iron-rich alumino-borosilicate glasses for nuclear waste forms with different Fe^{3+}/Fe^{2+} ratio. The coordination numbers and other detailed structural analyses were performed to investigate their roles and the competitions between the B, Al, and Fe^{3+} for charge compensation by Na and Fe^{2+} cations.

2. Methodologies and Simulation Details

MD simulations were carried out using parallel general purpose MD simulation package DL_POLY 2.20 developed by Smith and Forester from the Daresbury Laboratory of UK[56].In this work, seven glass compositions with different concentrations of FeO to Fe_2O_3 ratios, representing various redox ratios from pure ferric to pure ferrous, were studied by using MD simulations. The initial structure (with around 10,000 atoms) was randomly generated with minimum short distances among the atom pairs in a cubic simulation box. The number of atoms of each species and simulation box dimension for each of the glass compositions are provided in Table S1. The initial density used was the experimental value (2.66 g/cm^3) of the base glass composition FNAB. The simulation box was then gone through a simulated melt and quench

process[57]. Each system was heated to 6,000 K for 100,000 steps using the canonical ensemble (NVT) to fully melt the initial structures. It was then quenched to 300 K gradually with a cooling rate of 5K/ps, also under the NVT ensemble with the Berendsen thermostat.[56] A subsequent relaxation under the isobaric, isothermal (NPT) ensemble with the Berendsen thermostat and borostat[56] was performed under ambient pressure for 100,000 steps. A final production run under the NVE ensemble at 300K was performed to collect data for structural analysis. The cut-off distance for short-range interaction was 8 Å. For long-range interactions, Ewald sum method was used with a relative precision of $1x10^{-6}$ and a cut-off distance of 10 Å. Integration of the equations of motion using Verlet Leapfrog algorithm was performed where a time step of 1 femtosecond (fs) was adopted.

The partial charge pairwise potentials consist of a short-range Buckingham and a long-range Coulomb term with parameters refined by Du and Cormack[58] and with recent addition of boron oxide related parameters by Deng and Du[55]. The combined expression of the potential has the form as Eq.1. To better describe the partial covalence and partial ionicity of the chemical bonds existing in these kind of systems, partial charges of the ions are used in the Coulombic part of the potential.

$$V(r_{ij}) = \frac{Z_i Z_j e^2}{4\pi\varepsilon_o r_{ij}} + A_{ij}\cdot\exp(-r_{ij}/\rho_{ij}) - C_{ij}/r_{ij}^6 \quad (1)$$

where r_{ij} stands for the interatomic distance between two ions i and j; A, ρ, and C are the different parameters for Buckingham term. The partial atomic charge and parameters for short range interactions are listed in Table 1. Corrections of the Buckingham potential was used to avoid the overriding of the power term to the exponential term that caused problems at high temperature and initial high energy configurations at the interface. The following function form was used for the correction[59]:

$$V'(r_{ij}) = B_{ij} r_{ij}^2 + D_{ij} r_{ij}^n (2)$$

where B, D and n are parameters chosen to ensure the potential, force and first derivative of force to be continuous at the splicing distance r_s. The partial atomic charge and parameters for short range interactions are listed in Table 1[58]. Boron related parameters were recently developed and has a composition dependent A_{ij} parameter for B-O interactions to account for the effect of

glass composition on boron coordination change[59]. Details on how the B-O A_{ij} parameters are determined for multicomponent boroaluminosilicate glasses are described in Ref. 59. The parameters for ferrous and ferric species related pairs were recently developed based on cross fitting to the structures and mechanical properties of a number iron containing crystals.[27] The charge of ferrous iron is +1.2 and that of ferric iron is 1.8, scaled from their full charges based on the O^{2-} ion charge of -1.2. The partial ionic charges and potential parameters, including the Buckingham potential (Eq. 1) and short range correction terms (Eq. 2), are listed in Table 1.

The final 40,000 steps during the NVE production run were recorded every 50 steps for structural analyses such as the total correlation function (TDF), bond angle distribution (BAD), Q_n distribution and coordination number (CN). The first minima of the total correlation function were taken as the cut-off distances and used for the calculation for respective cation-oxygen pairs (Table S2). Details of these analyses can be found in reference such as Deng and Du[59].

Table 1 Atomic charges and Buckingham potential parameters[27,59]

Pairs	A_{ij} (eV)	ρ_{ij} (Å)	C_{ij} (eV.Å^6)	B_{ij} (eV.Å^6)	D_{ij}	n
$O^{-1.2}$-$O^{-1.2}$	2029.2204	0.343645	192.58	46.462	-0.32605	3.430
$Si^{2.4}$-$O^{-1.2}$	13702.905	0.193817	54.681	28.942	-3.0250	3.949
$B^{1.8}$-$O^{-1.2}$	Comp. dependent	0.171281	28.5	18.980	-4.1189	3.960
$Al^{1.8}$-$O^{-1.2}$	12201.417	0.195628	31.997	51.605	-10.073	3.193
$Na^{0.6}$-$O^{-1.2}$	4383.7555	0.243838	30.70	48.251	-4.7037	2.898
$Fe^{1.2}$-$O^{-1.2}$	11777.0703	0.207132	21.642	104.203	-32.110	2.670
$Fe^{1.8}$-$O^{-1.2}$	19952.29	0.182538	4.6583	260.9828	-340.739	2.115

Table 2Simulated glass compositions, densities and simulation cell sizes: 53.32SiO_2-9.12B_2O_3-23.93Na_2O-6.40Al_2O_3-(7.22-x)Fe_2O_3-2xFeO(mol%)

Name	***x value***	**SiO_2**	**B_2O_3**	**Na_2O**	**Al_2O_3**	**Fe_2O_3**	**FeO**	**Cell size Å**	**Final density**
FNAB	0	53.32	9.12	23.93	6.40	7.22	0	51.589	2.72
FNAB1	2.888	53.32	9.12	23.93	6.40	4.332	5.776	51.359	2.72

FNAB2	3.61	53.32	9.12	23.93	6.40	3.61	7.22	51.378	2.72
FNAB3	4.332	53.32	9.12	23.93	6.40	2.888	8.664	51.196	2.70
FNAB4	5.054	53.32	9.12	23.93	6.40	2.166	10.108	51.159	2.71
FNAB5	5.776	53.32	9.12	23.93	6.40	1.444	11.552	51.074	2.71
FNAB6	7.22	53.32	9.12	23.93	6.40	0	14.440	50.203	2.64

To investigate the iron redox ratio effect, we used a model borosilicate nuclear waste glass composition in which iron oxide was gradually reduced from 100% ferric to majority ferrous. Simulated glass compositions together with final density and cell parameter (for cubic simulation cells) are shown in Table 2. The glass compositions are 53.32SiO_2-9.12B_2O_3-23.93Na_2O-6.40Al_2O_3-(7.22-x) Fe_2O_3-2xFeO (x=0-5.776). It is worth noting that the 2x factor was used for FeO to maintain total iron constant, considering the 2:1 ratio of iron in Fe_2O_3 and FeO, while oxygen amount changes due to the redox reactions.

3. Results

3.1 Validation of the potential parameters

The developed iron potential parameters (Table 1) are used to calculate the structure and properties of several iron oxide and iron silicate minerals to validate the the potentials for iron oxide containing systems with both iron oxidation states. Comparison of the calculated and experimental cell parameters, bond distances, elastic properties are shown in Table 3. The results show that the potential is capable of describing iron oxides crystal structures[57] with high accuracy with <0.1% difference in cell parameters. Also, the iron-oxygen bond distances for both ferric and ferrous species are in good agreement with experiments for both 4- and 6-fold coordination. The calculated mechanical properties such as elastic moduli are also in good agreement with the available values from DFT calculations[58]. These results show that the partial charge potentials for iron related species can handle both iron oxidation states and in various coordination environments, which are essential as a variety of coordination states can exist in glass structures.

Table 3 Comparison of simulated (Sim, this work) and experimental structures and properties (from experiments or DFT calculations)[60,61] for iron oxide and silicates crystals. Unit cell parameters, Fe^{2+}-O, Fe^{3+}-O, Si-O bond distance range and coordination number (in [ ]), bulk (K), shear (G) and Young's (Y) moduli are compared.

Name (space group)	FeO (C2/m)		Fe_2O_3 (R-3/C)		Fe_3O_4 (Fd-3m)		Fe_2SiO_4 (Pnma)		$FeSiO_3$ (C2/c)	
	Sim.	Exp.	Sim	Exp.	Sim	Exp.	Sim	Exp.	Sim	Exp.
a, b, c (Å)	5.340/ 3.083/ 5.340	5.345/ 5.082/ 5.340	5.054/ 5.054/ 13.931	5.104/ 5/104/ 13.913	8.543/ 8.543/ 8.543	8.533/ 8.533/ 8.533	10.499/ 6.185/ 4.933	10.600/ 6.172/ 4.882	10.087/ 9.106/ 5.395	9.906/ 9.267/ 5.392
α, β, γ (°)	90.0/ 109.47/ 90.0	90.0/ 108.85/ 90.0	90.0/ 90.0/ 120.0	90.0/ 90.0/ 120.0	90.0/ 90.0/ 90.0	90.0/ 90.0/ 120.0	90.0/ 90.0/ 90.0	90.0/ 90.0/ 90.0	90.0/ 109.8/ 90.0	90.0/ 109.7/ 90.0
Volume ($Å^3$)	82.875	84.992	308.2	314.0	623.5	621.4	318.8	319.4	466.2	466.0
Fe^{2+}-O (Å) [4, 6]	2.180 [6]	2.087-2.264 [6]			2.025	1.912	2.146-2.323 [6]	2.152-2.255 [6]	2.084-2.315 [4, 6]	2.018-2.247 [4, 6]
Fe^{3+}-O (Å) [6]			1.959-2.125	1.980-2.127	2.053	2.097				
Si-O (Å) [4]							1.581-1.623	1.644-1.672	1.580-1.634	1.625-1.663
K (GPa)	157.3		197.2		164.5		114.9		98.2	
Y (GPa)	233.2/ 233.4/ 229.5	233[+]	262.8/ 262.8/ 315.9	246[+]	110.6	133[+]	127.5/ 162.0/ 232.6		253.6	
G (GPa)	94.3		89.3		68.4		59.9		57.7	

[+] from DFT+U calculations by Liao and Carter.[58]

3.2 The Structural Information of simulated FNAB glasses

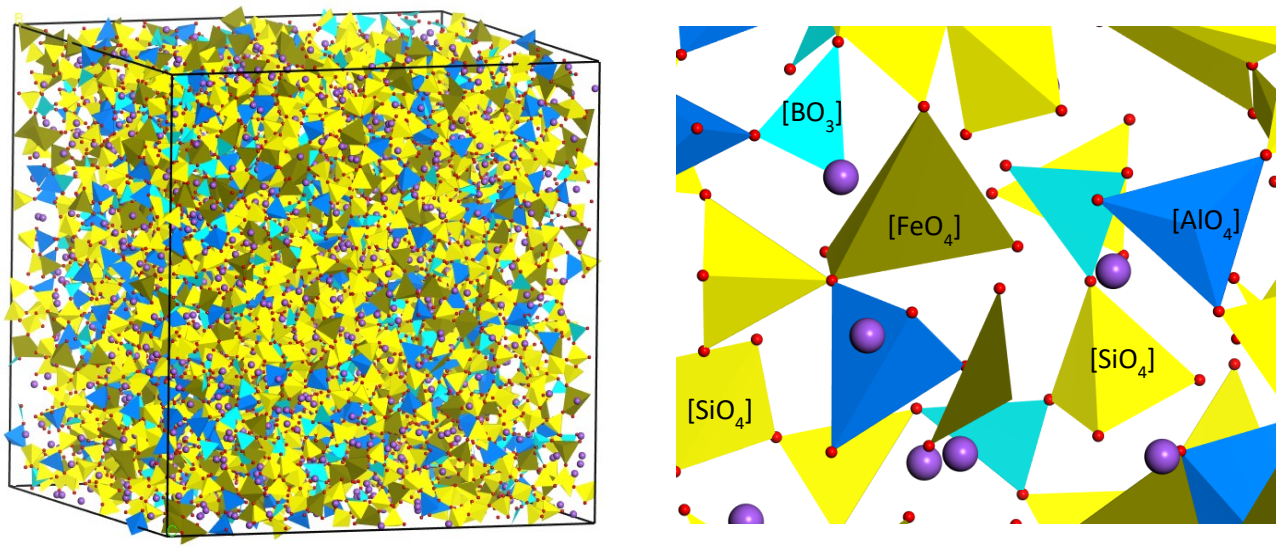

Figure 1 Snapshot of the MD simulated glass structure FNAB2 glass(a) full image of the simulation cell with ~10,000 atoms and cell parameter xxXyyXzz A (b) a zoomed in snapshot showing [SiO]$_4$ (yellow), [AlO]$_4$ (blue), [BO]$_x$ (light blue), [FeO]$_4$ (green) polyhedrons, Na (purple) and O (red).

Figure 1 shows the snapshots from the simulated structure of FNAB2 glass. This structure consists of polyhedra of the glass formers connected to each other by shared oxygen atoms at the corners. Total correlation functions (TDF) can effectively describe short-range structure in simulated glass compositions. Figure 2 shows the total correlation functions of the contributing pairs of simulated FNAB2 glass as a representative of FNAB series. The first major peak of TDF is the bond distance of that particular pair. Therefore, the bond distance of Si-O pair is located at around 1.61 Å representing the strong covalent nature of silicon with a well-defined first peak. This value agrees well with previous MD simulated aluminosilicate glasses and boroaluminosilicate glasses[62,63]. In addition, X-ray absorption spectra of silicate glass gives similar results with MD simulated ones obtained in this work [64]. The main peak of Al-O pair locates at around 1.77 Å, which is in good agreement with previous MD simulation results of sodium aluminosilicate glasses [55,65], as well as the experimental conducted XRD and EXAFS for both alumina and sodium aluminosilicate glasses[66]. Bond distances of Fe^{3+}-O and Fe^{2+}-O are around 1.86 Å and 2.07 Å respectively. The shorter bond length of Fe^{3+} with oxygen atoms can be explained by the greater degree of covalency of the Fe^{3+}-O bond and lower coordination

commonly found in amorphous materials[67]. Na-O bond distance is around 2.43 Å which consistently falls in the range obtained by X-ray absorption studies of sodium containing silica glasses[64]. Bond distances of the cation-oxygen pairs in simulated FNAB3 and FNAB5 glasses are summarized in Table 3 with previous experimental and *ab-initio* findings for comparison.

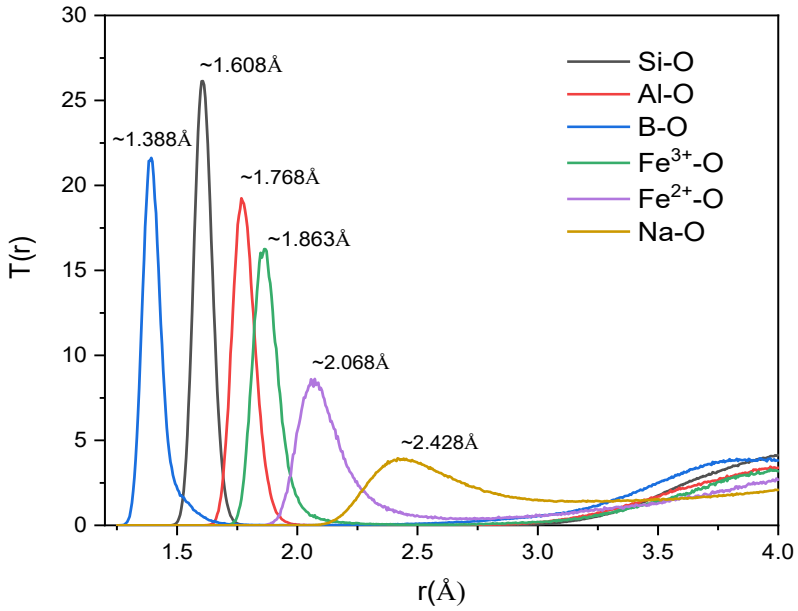

Figure 2 Total correlation functions of cation-oxygen pairs inFNAB2 glass

For example, B-O pair distribution plot contains two main peaks indicated in deconvoluted total correlation function of this pair in Figure 3 (a). The first peak locates at around 1.40 Å, representing the three-coordinated boron $^{[3]}$B, while for the four coordinated boron $^{[4]}$B, the corresponding peak locates at around 1.52 Å. These values are quite close to the ones obtained from experimental [68,69] and *ab-initio* calculations [70] for boron containing glasses. Figure 3 (b) shows the three and four coordinated boron species in FNAB glass series with varying redox ratio. With FeO/Fe_2O_3 substitution, the peak positions of three and four-coordinated boron remain unchanged but there is a systematic change in these peak intensities. This is a clear indication of the effect of Fe^{2+}/Fe^{3+} substitution on boron coordination which will be discussed thoroughly in the following section.

Table 2 Cation-oxygen bond distances in FNAB3/FNAB5 glasses

Cation-oxygen pairs	Bond Length, Å	Exp.	*ab initio*
Si-O	1.60/1.61	1.60-1.61[64]	1.64[1]
Al-O	1.77/1.76	1.77[66]	-
$B^{[3]}$-O	1.39/1.39	1.37-1.38[68,69]	1.37[70]
$B^{[4]}$-O	1.50/1.50	1.48-1.49[68,69]	1.47[70]
Fe^{3+}-O	1.86/1.85	1.89(tetra)/2.05(octa)[71]	-
Fe^{2+}-O	2.07/2.07	2.03(tetra), 2.17(octa)[71]	-
Na-O	2.43/2.44	2.30-2.43 [64], 2.46-2.62[66]	2.36-2.43[1]

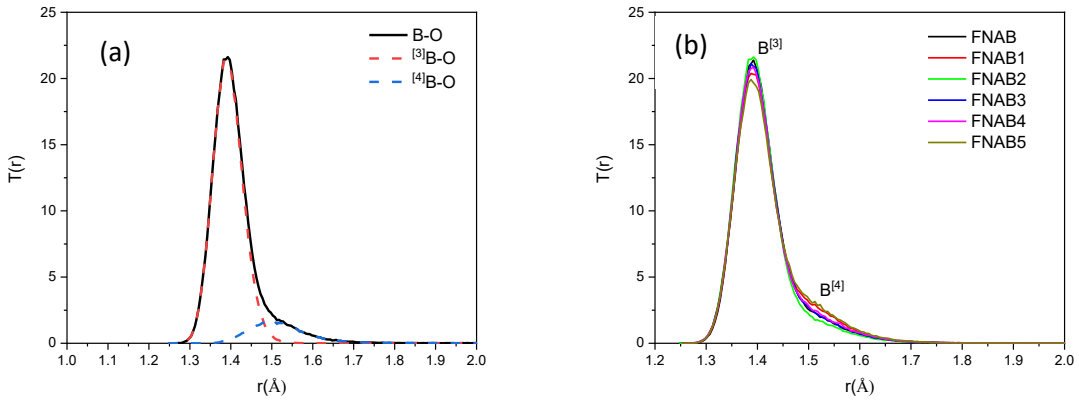

Figure 3 (a) Deconvoluted B-O total correlation function of simulated FNAB2 glass. Three and four-coordinated boron are shown in red and blue dashed line respectively and (b) total correlation functions of boron species in FNAB glass series

The coordination number distributions of cation-oxygen pairs in FBNA2 glass are demonstrated in Figure 4. Both silicon and aluminum are found to be typical fourfold coordinated, which agrees with previous MD studies for international simple glass (ISG), boroaluminosilicate and lithium aluminosilicate glasses[55,72,73]. For the Fe^{3+} species, the coordination number is similar to that of Si and Al, staying slightly higher than 4. Another important feature of the coordination distribution of Fe^{3+} is that, it has an increase than an elongated plateau region again followed by increment with distance which is very similar to a glass network formers' behavior. On the other hand, coordination distribution of Fe^{2+} is more like that of glass modifier – an overall increment with distance without showing any clear

plateau region. It is in accordance with previous studies where divalent iron is usually found to be network modifier and being five- to six-coordinated in most silicate glasses while for trivalent iron is considered to be a network former and four-coordinated[74]. Again,it can be observed from Figure 2, for the Fe^{3+} in FBNA2 glass, the high sharp peak locates at around 1.86 Å, close to that of Al, representing a glass former behavior. Interestingly, the Fe^{2+} species in FBNA glasses display broader peak than those of network formers (Si, B, and Al), while narrower peak than those of glass modifier (Na in this work), locating at around 2.07 Å.

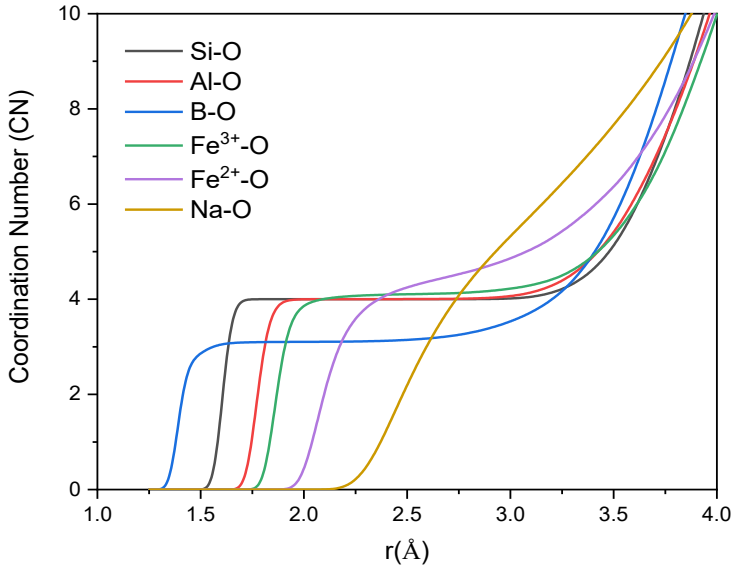

Figure 4 Coordination numbers (CN) of the cation-oxygen pairs in the simulated FNAB2 glass structure

3.3 Cation coordination distribution and average coordination number

Coordination environment captures the short-range local structure of the comprising elements of glass matrix. By integrating the first peak of partial pair distribution function coordination number is obtained and it is defined as $\int_0^{r_c} 4\pi r^2 \rho(r) dr$. Here, r_c is the cut-off value for each pair which can be obtained from the first minima of the corresponding TDF curve. For Si, Al, Fe^{3+}, B, Na, and Fe^{2+} the cut-off values were taken to be 2.25 Å, 2.35 Å, 2.45 Å, 1.85 Å, 3.31 Å, and 2.76 Å respectively. Oxygen coordination numberof the glass formers and glass modifiers for FNAB to FNAB5 samples are calculated and summarized in Table 4-9.

3.3.1 Coordination environment of Si, Al, Fe^{3+}

Table 3 and 4 report the coordination distribution and mean coordination number of Si and Al respectively. The average oxygen coordination of silicon in all the glass compositions is four i.e. it is the tetrahedral glass forming units as found in silicate and aluminosilicate melts and glassesfrom experimental results [75,76] and various MD studies[63,65].Aluminum is found to be mostly four-fold coordinated, but minute amount of five-coordinated Al is also observed in all the glass compositions. This is in well accordance with previously reported experimental results [77,78].It is worth taking into consideration that, for both Si and Al, the coordination environment is not significantly affected by the FeO/Fe_2O_3 substitution i.e. iron redox ratio.

The coordination number results of Fe^{3+} is reported in Table 5. The reported values are average standard deviation are from three parallel simulations for each composition. It can be seen that, Fe^{3+}ismostly four-coordinated. This is again an indication that, Fe^{3+}ions are able to connect as three-dimensional tetrahedral units similar to the characteristics of a glass network former. Compared to Al^{3+}, the amount of five-coordinated Fe^{3+} are much higher at all five samples. More importantly, the amount of over-coordinated Fe^{3+} were affected by the concentration of Fe^{2+}. Throughout the FNAB series, as the concentration of Fe^{2+} increases, the presence of over coordinated Fe^{3+} first increases and then increases and finally decreases to a lower amount.

Table 3 Coordination distribution and mean coordination of Si

Glass ID	4	5	Avg Coord.
FNAB	99.94±0.01	0.06±0.01	4.00±0.00
FNAB1	100±0.00	0.00±0.00	4.00±0.00
FNAB2	100±0.02	0.00±0.02	4.00±0.00
FNAB3	100±0.00)	0.00±0.00	4.00±0.00
FNAB4	100±0.00	0.00±0.00	4.00±0.00
FNAB5	100±0.00	0.00±0.00	4.00±0.00
FNAB6	99.98±0.02	0.03±0.03	4.00±0.00

Table 4Coordination distribution and mean coordination of Al

Glass ID	4	5	Avg Coord.
FNAB	99.97±0.51	0.02±0.49	3.99±0.01
FNAB1	99.44±0.20	0.50±0.23	4.00±0.00
FNAB2	99.84±0.48	0.17±0.47	4.00±0.01
FNAB3	99.49±0.65	0.51±0.64	4.00±0.01
FNAB4	99.67±0.15	0.32±0.15	4.00±0.00
FNAB5	99.63±0.35	0.37±0.35	4.00±0.00
FNAB6	98.75±0.22	1.25±0.23	4.02±0.01

Table 5 Coordination distribution and mean coordination of Fe^{3+}

Glass ID	4	5	6	Avg Coord.
FNAB	93.33±3.58	6.59±3.57	0.03±0.09	4.09±0.02
FNAB1	94.14±3.90	5.46±4.07	0.14±0.05	4.11±0.02
FNAB2	90.09±2.89	9.76±2.96	0.15±0.08	4.10±0.03
FNAB3	89.72±3.35	10.24±3.38	0.04±0.09	4.09±0.04
FNAB4	93.82±5.49	6.18±5.45	0.00±0.05	4.13±0.02
FNAB5	97.62±6.11	2.39±5.70	0.00±0.49	4.14±0.03
FNAB6	-	-	-	4.09±0.02

3.3.2Boron coordination and fraction of four-coordinated B (N_4)

Boro- and aluminoborosilicate glasses exhibit non-linear composition dependence on the glass compositions which is known as boron anomaly[79–81]. As proven by the studies of solid-state NMR, this is related to the conversion of three ($^{[3]}$B) to four -coordinated boron ($^{[4]}$B) – at the initial stage of modifier oxide (Na_2O,CaO etc.) addition $^{[3]}$B convert to $^{[4]}$B, then a plateau region appears and lastly with further increase of modifier oxide $^{[4]}$B breaks up to generate non-bridging oxygens(NBO) first on B and then on Si[10,82,83]. Since the findings from the preceding sections suggest FeO to be of glass modifier's role, it would be interesting to observe how the variation in redox ratio affect the fraction of four-coordination boron (N_4).

Table 7 reports the percentage of three- and four-coordinated boron in FNAB glass series. Different from other glass formers, FeO concentration has higher effect on boron species. It is concluded that an increase in the FeO concentration decreases the concentration of three coordinated boron and increases the concentration of the four coordinated ones. $^{[3]}$B concentration declines from 87.70% for FNAB to 78.90% for FNAB6, while the $^{[4]}$B concentration increases from 12.30% for FNAB to 21.10% for FNAB6. Figure 5 shows the comparison of the fraction of four coordinated boron obtained by MD simulations with the ones found theoretically. It can be observed that, the trend is more of less with an overall increment of boron N_4 with the addition of Fe^{2+} even though there is slight disagreement at some points. Ming-Tai *et al.*[84] reported that charge compensator prefers Al to B in sodium-alumino-boro glasses. Our results confirmed that at a fixed amount of alumina, increasing of Fe^{2+}, which denotes to a network modifier greatly increased $^{[4]}$B concentration.

Table 6 Coordination distribution and mean coordination of B

Glass ID	3	4	Avg Coord.
FNAB	87.70±2.84	12.30±2.84	3.12±0.03
FNAB1	85.07±1.19	14.93±1.19	3.14±0.02
FNAB2	89.96±5.04	10.05±5.03	3.10±0.05
FNAB3	87.39±2.23	12.61±2.23	3.12±0.02
FNAB4	86.15±1.23	13.86±1.22	3.14±0.01
FNAB5	83.18±1.22	16.82±1.22	3.16±0.02
FNAB6	78.90±2.39)	21.10(±2.39)	3.21±0.03

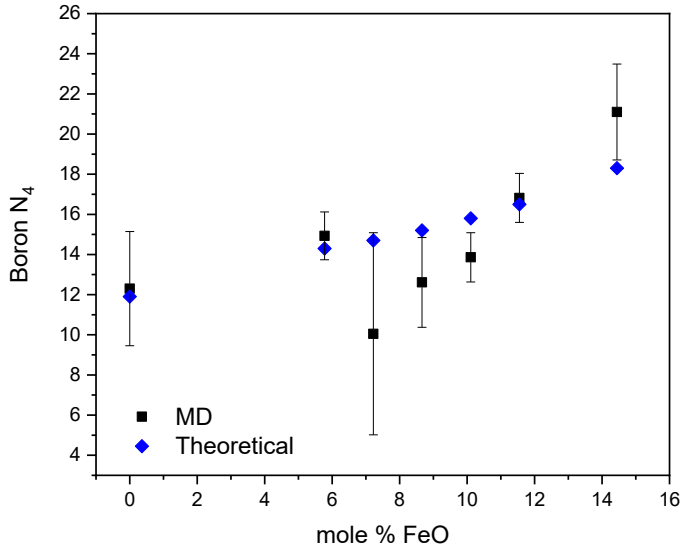

Figure 5 Coordination number for B species in FNAB glass series from MD simulations and theoretical calculations (modified Dell and Bray model)

3.3.3 Distribution of coordination number of the glass modifiers (Na, Fe^{2+})

As discussed earlier from Figure 4, glass modifiers show broader distribution of oxygen coordination number. Table 7 summarizes the oxygen coordination number Na and it varies between 5 to 8 coordination mostly resulting in an average of ~6.5. This is in well accordance with the Na coordination obtained from MD results in bioactive [85] and from DFT-GIPAW calculations for borosilicate glasses[1]. There is an increase of average coordination number for Na from 6.43 to 6.59. For Fe^{2+} species (Table 7), on the other hand, the main contributions are from four and five-coordinated Fe^{2+}, with significant amount of six-coordinated and small number of three-coordinated ones. The average coordination number of Fe^{2+} locates at around 6.54. There is a slight decrease in the average coordination of Fe^{2+} with increase of its concentration.

Table 7 Coordination distribution and mean coordination of Na

Glass ID	5	6	7	8	Avg Coord.
FNAB	18.11±4.23	29.58±1.08	28.93±2.53	15.08±2.40	6.43±0.20
FNAB1	17.31±2.89	31.83±2.43	29.97±1.90	14.31±2.87	6.44±0.17

FNAB2	16.64±2.77	32.07±2.35	29.71±1.76	14.14±2.58	6.43±0.16
FNAB3	14.89±1.16	30.27±0.76	31.27±0.65	14.96±1.61	6.55±0.09
FNAB4	14.79±1.20	32.22±1.20	30.73±1.06	15.43±0.60	6.56±0.09
FNAB5	14.35±1.75	29.55±0.23	32.74±1.39	15.48±1.00	6.59±0.07
FNAB6	9.96±0.51	29.40±0.61	33.50±0.95	19.15±0.64	6.77±0.02

Table 8 Coordination distribution and mean coordination of Fe^{2+}

Glass ID	3	4	5	6	Avg Coord.
FNAB	-	-	-	-	-
FNAB1	1.19±0.34	47.02±6.08	42.86±4.81	7.74±1.71	4.60±0.08
FNAB2	0.47±0.55	55.9±7.10	37.44±5.20	6.16±1.71	4.49±0.08
FNAB3	1.19±0.46	51.7±3.85	37.55±4.88	9.49±2.30	4.55±0.04
FNAB4	1.01±0.58	52.7±3.72	36.82±3.25	8.78±1.79	4.55±0.05
FNAB5	0.29±0.30	51.76±0.51	40.00±0.74	7.94±0.45	4.56±0.01
FNAB6	0.47(±0.49	37.94±2.57	47.54±2.39	13.82±2.23	4.75±0.04

3.4 Bond angle distribution (BAD)

Bond angle distribution (BAD) is an effective way to describe the short-range structure changes. Angle formed inside glass forming polyhedrons (O-X-O, where X stands for glass former) and angle formed by two different polyhedrons (X-O-X) connected by oxygen atom are analyzed.O-X-O BAD is used to describe the regularity of the glass former tetrahedrons whereas the X-O-X BAD describes the tetrahedron connectivity[86,87]. The two kinds of BAD were

analyzed for FNAB glasses and were demonstrated in Figure 6 and 7 respectively.

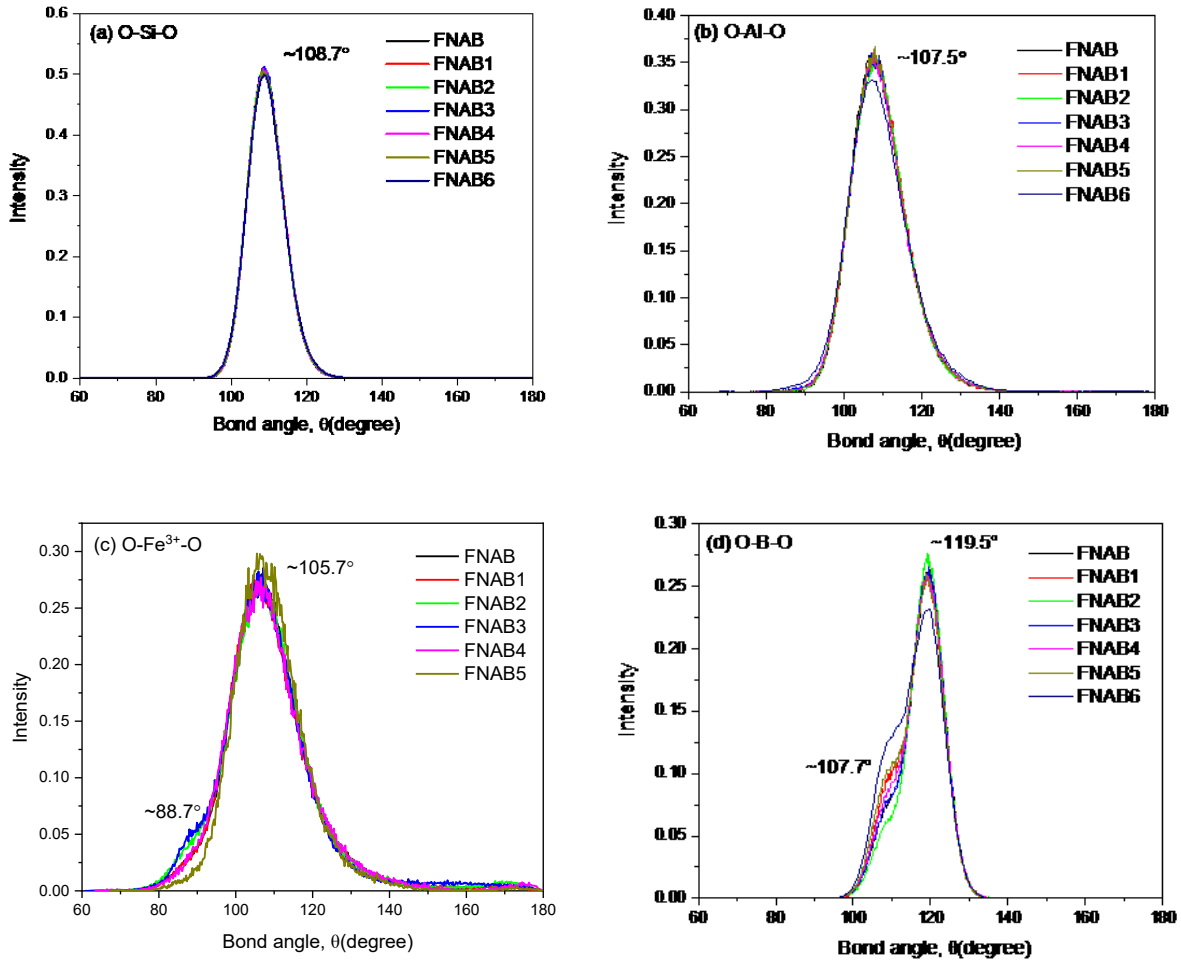

Figure 6 Bond angle distribution of the glass formers with surrounding oxygen atoms

It can be observed from Figure 6 that the BAD of O-Si-O, O-Al-O, and O-Fe^{3+}-O show peaks at around 108.7°, 107.5°, and 105.7°, respectively. These values are close to the theoretical tetrahedral angle109.5° and it indicates the tetrahedral geometry of [SiO_4], [AlO_4], and [FeO_4]. The result of O-Si-O agrees well with the experimental data based on high-energy X-ray diffraction and neutron scattering data[88,89]. The BAD of O-Al-O, shown in Figure 6(b), is relatively wider than that of O-Si-O, which agrees well with previous simulation results in sodium-aluminosilicate and boroaluminosilicate glasses[55,90]. For O-Fe^{3+}-O, the BAD gives an even broader peak, locating at around 105°. The narrower BAD and closer peak value to the

optimal tetrahedron angle of Si when compared to Al and Fe^{3+}indicate its well-defined first coordination shell as a result of high field strength of Si^{4+} ions[85]. Interestingly, substitution of FeO/Fe_2O_3 did little effect on the BAD of These three species. For O-Si-O and O-Al-O, the six curves in Figure 6(a) and 6(b) overlap with each other. For O-Fe^{3+}-O, only peak intensity changes to some extent since Fe^{3+} ions are reduced by the gradual introduction of Fe^{2+} (Figure 6(c)).Also, there is a shoulder at around 90° which is likely to be formed because of the triangular bi pyramidal shapes of five-coordinated units. Bond angle distribution of O-B-O in FNAB glass series are shown in Figure 6(d) and it exhibits interesting behavior. These plots have two main peaks; the first one located at ~107.5°which refers to four-coordinated B tetrahedrons, and the second peak located at 119.5° corresponds to three-coordinated B which has a triangular shape. Different from other three glass formers, the increase of Fe^{2+} concentration caused the changes on intensities of these two peaks. This is due to the variation of three- and four-coordinated B concentrations. This result agrees well with the T(r)(Figure 3) and coordination number distribution of B-O pair (Table 7). As shown in Figure 6(d), with increasing Fe^{2+}, the peak intensity of three-coordinated B decreases while four-coordinated B increases.

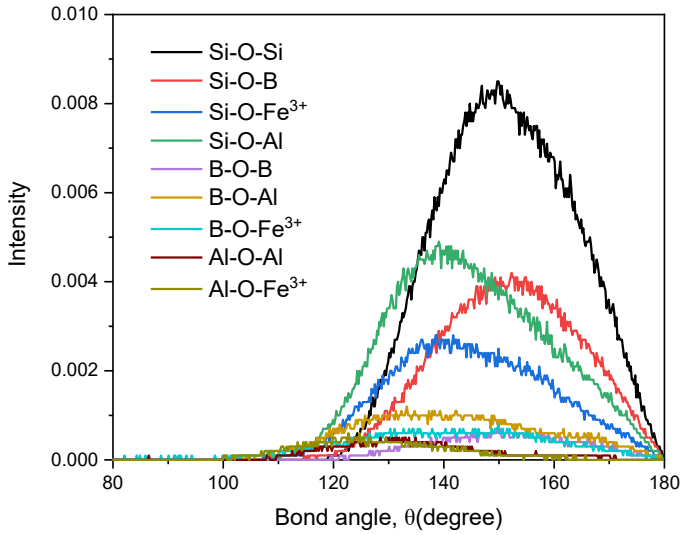

Figure 7 Inter-polyhedron bond angle distribution in simulated FNAB2 glass structure

Figure 7 shows the inter-polyhedron BAD among different glass forming units. These polyhedrons are connected to each other by an oxygen atom at the center. The peak intensity of a

certain bond angle also indicates the probability of that particular linkage formed by a pair of polyhedrons. It can be observed that, Si-O-Si BAD is of highest intensity in these glasses therefore it is the most favorable linkage and occurs abundantly. Si-O-Al BAD is the next favorable linkage formed in these glasses. In this study, the concentration of SiO_2 is around eight times greater than that of Al_2O_3. Therefore, there is higher probability of Si-O-Si linkage occurring compared to that of Si-O-Al linkage. Another interesting observation can be made from Figure 7: the presence of Al-O-Al linkage which might seem like the violation of Lowenstein's aluminum avoidance principle that states, with greater Si/Al ratio, Al-O-Al bond is unlikely to happen[91,92]. Al-O-Al linkage was also observed in the findings from other MD simulation results [63,93]. The violation of aluminum avoidance rule was suggested to be caused by introduction of higher field strength glass modifier in the matrix such as Fe^{2+} in this study[94].

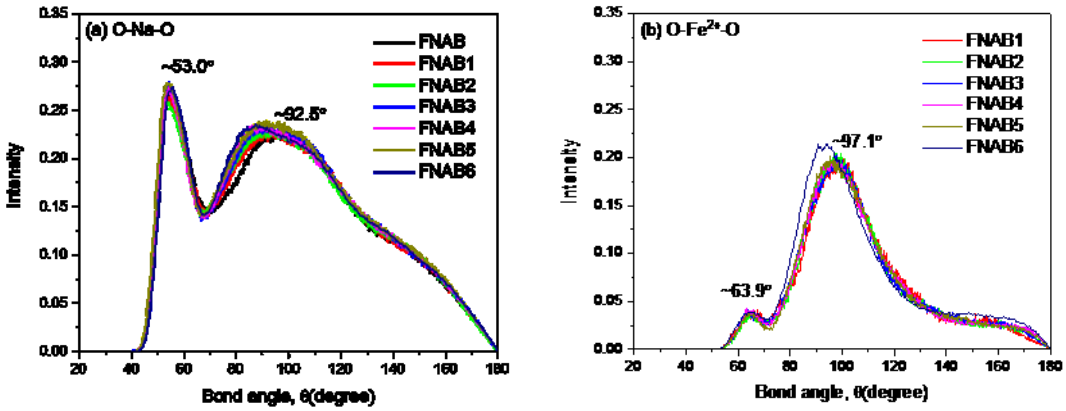

Figure 8 Bond angle distribution of (a) O-Na-O and (b) O-Fe^{2+}-O

Figure 8 shows the BAD of glass modifiers (Na, Fe^{2+}) for six different glass compositions in FNAB systems. Overall, these BADs do not show significant variation with changing redox ratio. BAD for sodium ions extends from 40° to 180° and it has two major peaks: at around ~53° and 93°. Similarly, for ferrous iron extends from ~55° to 180° forming two prominent peaks at ~64° and 97.1°. This characteristic of modifier's BAD was well explained by Xiang and Du[85]considering the contribution of bridging (BO) and non-bridging oxygen (NBO) to the BADs. For both of the modifiers, the peak at around 90° occurs by the octahedral geometry of the connection between two NBOs from two different glass forming polyhedra such as [SiO_4],

[AlO_4] etc. in this study. On the other hand, the peak at ~60° forms by oxygen atoms sharing same polyhedrons. The partitioned BAD in Figure 9 reveal the contribution of BO and NBO to the overall distribution. It can be observed that, for sodium, the peak at lower angle is mostly contributed by BO-Na-BO whereas the higher angle peak is contributed by BO-Na-NBO and BO-Na-BO. For ferrous iron, the peak at lower angle is not of as high intensity as sodium and contributed by BO-Fe^{2+}-NBO whereas the high angle peak is formed by NBO-Fe^{2+}-NBO. Therefore, it can be suggested that, Fe^{2+} has greater level of association with NBO in first coordination shell that that of Na.

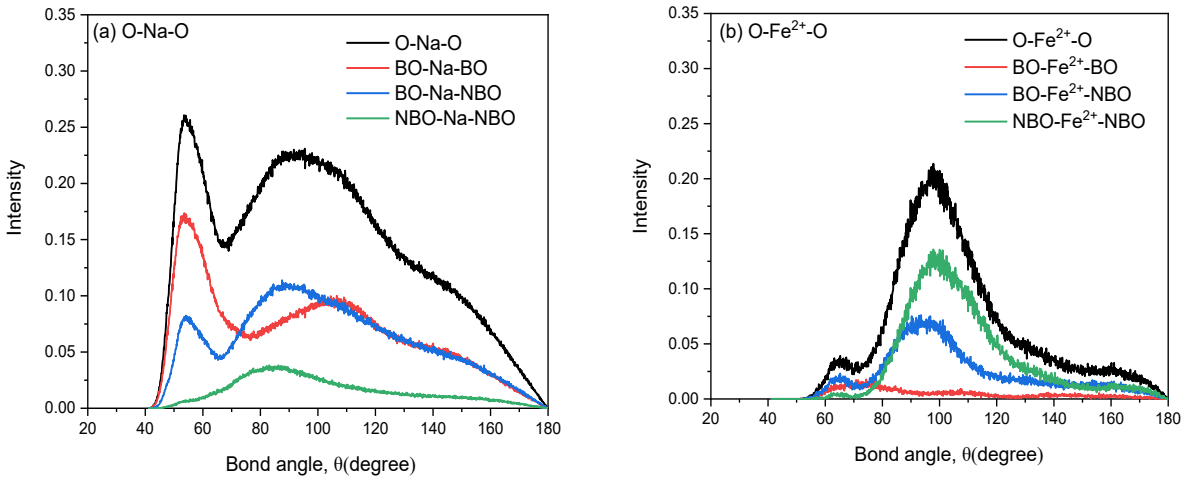

Figure 9 Contribution of BO and NBO in bond and distribution of (a) O-Na-O and (b) O-Fe^{2+}-O in simulated FNAB2 glass structure

3.5 Preference of Na and Fe^{2+} by Al, Fe^{3+}, and B

When being four-fold coordinated, the 3+ charged cations will have a negative charge on the [MO_4]- (M=Al^{3+}, B^{3+} and Fe^{3+}) tetrahedron, assuming all the oxygen being bridging oxygen and the tetrahedron entering the silicate network by linking to [SiO_4] through common bridging oxygens. As we have two types of modifier cations: Na^+ and Fe^{2+}, it would be intriguing to determine which one is preferred to play the charge compensation role on these 3+ cations. For this purpose, we have calculated the cation-cation pair distribution functions (PDF) and the cation preference ratios[95].

PDFs of the glass formers (Na, Fe^{2+}) were obtained and reported in the Figure 10. In Figure 10(a), the overlapping peaks of the PDFs of Na with different glass formers suggest a close competition among the glass formers to be charge compensated by sodium. From Figure 10(b), it can be observed that, the PDF peaks of Al and Fe^{3+} by Fe^{2+} is almost of similar intensities. Therefore, it can be concluded that Fe^{2+} ions are charge compensating Al and Fe^{3+} with similar level of preference. Another way to look at the charge compensating tendency of the modifier is to consider the number of a particular glass former ion around each of the glass modifiers. It can be calculated as a ratio denoted as 'R' which has an expression as the following [95]:

$$R^{a}_{b/c} = \frac{CN_{a-b}}{CN_{a-c}} \times \frac{N_c}{N_b}$$

in which, 'a' stands for a particular glass modifier (Na or Fe^{2+}), 'b' and 'c' denote glass modifiers (Al, B, and Fe^{3+}). If R>1, 'a' prefers 'b' over 'c' and for R<1, 'c' is more preferred by 'a'. When R is around 1, there is a statistical distribution of 'b' and 'c' around 'a' according to the number density of the cell and there is no particular preference of 'a' toward 'b' or 'c'. The calculated values are reported in Table 9. Between Al and Fe^{3+}, Na charge compensate Fe^{3+} first and between Al and B, Na charge compensate Al first in all the glass compositions. Therefore, the sequence of preferential charge compensation by Na is $Fe^{3+} \geq Al > B$. Since the calculated values of R for charge compensation by Na between Al and Fe^{3+} are close to 1, competition between these two glass formers for Na is almost similar. This is also in accordance with the other observation of this study where Al and Fe^{3+} are found to be of similar nature. In case of Fe^{2+}, again Fe^{3+} is first charge compensated, then Al and finally B. Therefore, the sequence is same as Na. The preferential sequence of Fe^{2+} for charge compensation is also shown in Table 9. The results show that Fe^{2+} has larger preference for Fe^{3+} than B, it also has preference for Al^{3+} than B, while between Fe^{3+} and Al, the preference of Fe^{3+} is higher. Hence the preferential sequence of Fe^{2+} for charge compensation is $Fe^{3+} \geq Al > B$ and the highest preference is Fe^{3+}.

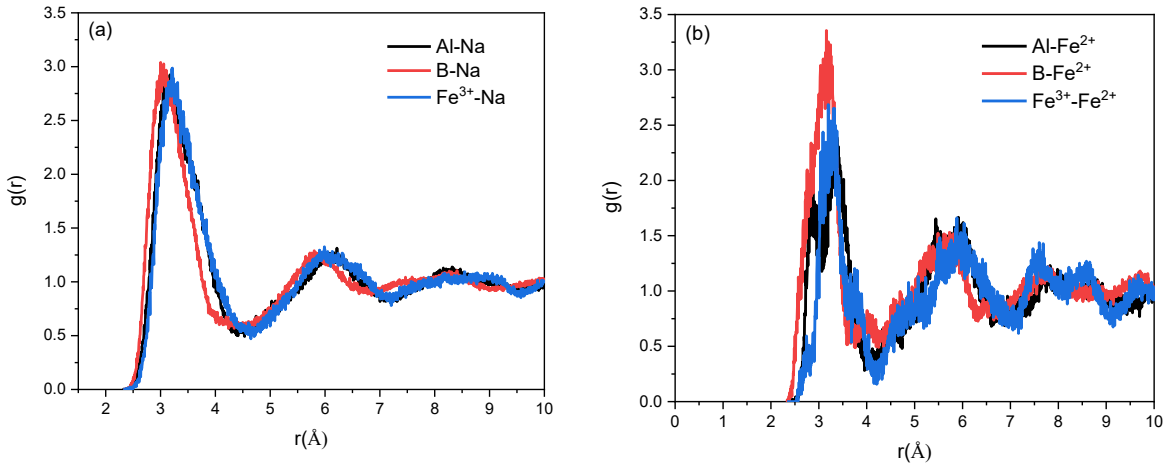

Figure 10 Partial distribution functions of (a)Na and (b)Fe^{2+} with different glass formers in simulated FNAB2 glass structure

Table 9 Charge compensation preference of Na and Fe^{2+} for Al, Fe^{3+}, and B in FNAB glasses series

Glass ID	$R^{Na}_{Al/B}$	$R^{Na}_{Fe^{3+}/B}$	$R^{Na}_{Fe^{3+}/Al}$	$R^{Fe^{2+}}_{Al/B}$	$R^{Fe^{2+}}_{Fe^{3+}/B}$	$R^{Fe^{2+}}_{Fe^{3+}/Al}$
FNAB	1.20	1.22	1.12	-	-	-
FNAB1	1.19	1.23	1.04	1.45	2.11	1.45
FNAB2	1.16	1.24	1.07	1.44	2.52	1.75
FNAB3	1.45	1.27	1.10	1.45	3.16	2.18
FNAB4	1.12	1.58	1.03	1.45	4.22	2.90
FNAB5	1.15	1.26	1.10	1.44	6.31	4.37
FNAB6	1.58	-	-	1.08	-	-

3.6 Oxygen speciation

The concentration of bridging and non-bridging oxygen in FNAB glass series were summarized in Table11. The high concentration of bridging oxygen (88.47%) indicates that the

baseline FNAB glass (without Fe^{2+}) is a highest network former containing glass, with 10.15% of non-bridging oxygen and small amount of tri-bridging oxygen. The percentage of bridging oxygen around the glass formers is decreasing from 88.47% to 72.91% with increasing Fe^{2+}content, while the non-bridging oxygen shows the opposite trend. Since the glass compositions studied have a fixed amount of Na_2O, and the total concentration of $[Al_2O_3+Fe_2O_3+B_2O_3]<[Na_2O]$, Na is only acting as a charge compensator for Al, Fe^{3+} and B[94]. Therefore, it is only because of the Fe^{2+} the non-bridging oxygen is being generated. Therefore, Fe^{2+} ions play the role of breaking the network linkages by generating extra non-bridging oxygens which again confirms its role as a glass modifier. Figure 11 shows the partial distribution functions (PDF) of these glass modifiers with associated non-bridging oxygen. Since PDFs are calculated by normalizing the concentration of the corresponding components, higher intensity of the Fe^{2+}-NBO than Na-NBO peak indicates that, greater the number of NBOs are conglomerated with Fe^{2+} than Na for the equal amount of these glass modifiers.

Table 10 Oxygen coordination in FNAB glass series (%)

Glass ID	1	2	3
FNAB	10.15(±0.40)	88.47(±0.29)	1.38(±0.18)
FNAB1	18.11(±0.27)	81.45(±0.35)	0.42(±0.19)
FNAB2	20.73(±0.59)	78.69(±0.63)	0.52(±0.04)
FNAB3	22.80(±0.28)	76.76(±0.22)	0.43(±0.08)
FNAB4	24.84(±0.13)	74.79(±0.16)	0.27(±0.04)
FNAB5	26.83(±0.19)	72.91(±0.10)	0.12(±0.07)
FNAB6	31.32(±0.24)	68.34(±0.28)	0.23(±0.07)

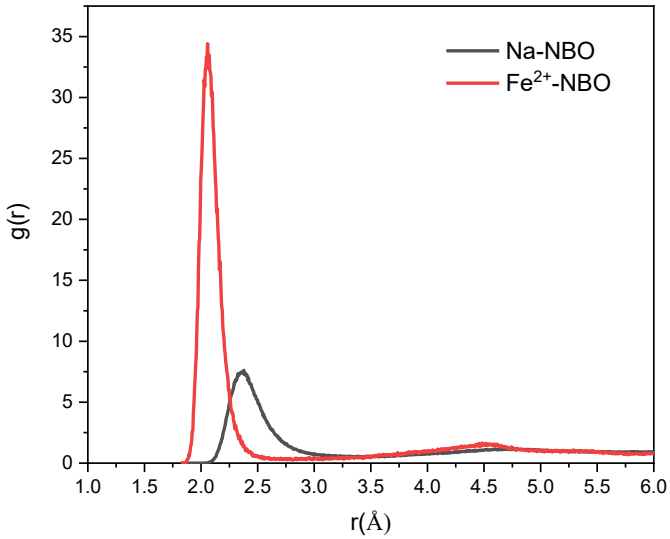

Figure 11 Partial distribution function of Na and Fe^{2+} with associated non-bridging oxygens (NBO) in simulated FANB2 glass

3.7 Q_n distribution of Silicon, Boron, Aluminum, and Iron (Fe^{3+})

In glassy or amorphous materials, the statistical distribution of various structural motifs on different scales is represented by Q_n. Q_n refers to the glass forming units where 'n' (~0-4) is the number of bridging oxygens per tetrahedron[96]. It is a medium range structure information and sheds lights on the glass network. The Q_n distributions of silicon, aluminum, ferric iron, and boron were studied in order to analyze the medium range behavior of FNAB glasses and reported in Table 12-15. It can be observed that the preferred species for these three species are Q_4, which indicates high connectivity of network formers. In addition, for Si, Al, and Fe^{3+} species, the percentage of Q_4 decreases as the Fe^{2+} content is increasing, whereas the percentage of Q_3 decrease. Furthermore, the Q_4 species of Si decreases dramatically from 72.96% to 43.53%, indicating high Fe^{2+} content decreases the probability to form linkages between Si and other network-formers and resulting the increase of Q_2 and Q_3 species.Q_1 and Q_2 species, they result from the non-bridging oxygen existing in these glasses. In addition, the existence of $Q_5$of Al and Fe^{3+} indicate the presence of five-coordinated Al in FNAB glasses. For Fe^{3+}, it suggests that majority are connected to other network formers.

Table 11Q_n distribution of Si (%)

Glass ID	Q_1	Q_2	Q_3	Q_4
FNAB	0.00	2.58	24.42	72.96
FNAB1	0.45	6.93	35.29	57.26
FNAB2	1.16	7.67	37.51	53.67
FNAB3	0.80	10.89	40.58	47.73
FNAB4	1.00	11.18	43.88	43.87
FNAB5	1.62	13.60	41.19	43.53
FNAB6	3.10	16.40	44.02	36.45

Table 12Qn distribution of Al (%)

Glass ID	Q_3	Q_4	Q_5
FNAB	1.90	98.08	0.02
FNAB1	10.49	88.74	0.50
FNAB2	12.84	86.46	0.17
FNAB3	9.83	89.13	0.51
FNAB4	12.75	86.46	0.28
FNAB5	14.88	83.97	0.35
FNAB6	20.27	77.68	1.25

Table 13Q_n distribution of Fe^{3+} (%)

Glass ID	Q_3	Q_4	Q_5	Q_6
FNAB	2.47	90.92	6.59	0.03
FNAB1	5.82	88.59	5.46	0.14
FNAB2	9.83	80.63	9.31	0.15
FNAB3	8.24	82.65	9.07	0.04
FNAB4	9.31	83.78	6.13	0.00
FNAB5	11.61	85.98	2.39	0.00

FNAB6	-	-	-	-

Table 14 reports the Q_n distribution of boron. The majority parts are Q_3 and Q_4, corresponding to three- and four-coordinated B respectively. Here, increasing Fe^{2+} leads to increase of Q_1 and Q_2 concentrations. Therefore, with introduction of extra Fe^{2+} more non-bridging oxygens are generated. In addition, the increase of Fe^{2+} content results in an increase trend of Q_4 and decrease trend of Q_3 species. This is due to the availability of more network modifier to charge compensate the B, corresponding the results of coordination number change of B which resulted in the increase of boron N_4which is also in accordance with the result obtained from Figure 5. Therefore, increase of Fe^{2+} has two-fold effect on the local environment of boron: it increased the non-bridging oxygen around it and also charge compensate to produce four-coordinated boron.

Table 14 Q_n distribution of B (%)

Glass ID	Q_1	Q_2	Q_3	Q_4
FNAB	0.66	19.14	68.38	11.82
FNAB1	4.57	25.80	55.56	14.07
FNAB2	4.31	32.89	54.68	8.12
FNAB3	5.30	30.09	54.53	10.09
FNAB4	5.89	33.61	48.92	11.39
FNAB5	7.32	35.52	42.83	13.58
FNAB6	10.25	33.14	37.77	17.35

4 Discussions

4.1 Structures of the iron containing borosilicate glasses

From the obtained results, it can be observed that, even though the local structure and the coordination states of silicon, aluminum and ferric iron were not significantly affected by the modulation of redox ratio, boron coordination state are strongly influenced by the iron redox ratio. Our simulation results clearly show that Fe^{3+}plays the role as a glass former whereas Fe^{2+}

acts as a glass modifier, as demonstrated in Figures2, 4 and Table 6.The coordination number of the two iron species are compared in Fig. 12. It can be clearly seen that Fe^{3+} has over 90% four-fold coordination hence supporting the role of Fe_2O_3 a glass former in these and other silicate glasses. Fe^{2+}, on the other hand, has significant amount of five- and six-fold coordination. Fe^{3+}-O shows a well-defined first coordination shell and the accumulated coordination has a clear plateau. Together with majority (close to 90%) of the Fe^{3+} ions are four-fold coordinated, all these give evidence that Fe^{3+} mainly plays the role of a glass former. It is worth noting that Fe^{3+} can also occur in six-fold coordination which is generally observed in crystalline sodium iron silicates such as acmite ($NaFeSi_2O_6$)[67]. An earlier Mössbauer and neutron diffraction study suggested that both iron species are four-fold coordinated by oxygen, although longer Fe-O bond distance was found for the ferrous species than the ferric species[67] which is consistent with our simulation results (Table 2 shows that Fe^{2+}-O bond distance is 2.07 Å and Fe^{3+}-O bond distance is 1.86 Å). The experimental results also support that ferric oxide (Fe_2O_3) plays the role of an intermediate,[67] consistent with our findings. In this work, Fe^{2+} shows more of a typical modifier like characteristics: Fe^{2+}-O^{2-} pair distribution function is broader, lacks of a clear plateau of accumulated coordination and a significantly higher coordination than 4. The compositions designed was to keep other components of the borosilicate glass constant while only changing the redox ratio of iron oxide by gradually increasing the reduction of Fe^{3+}.

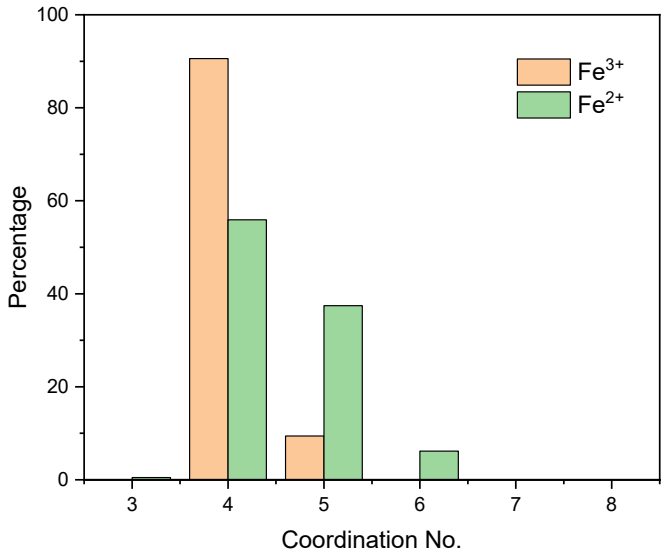

*Figure 12 Oxygen coordination number distribution around Fe^{3+} and Fe^{2+}*in FNAB2.

The redox ratio of iron oxide has significant effect on the glass structure, especially on the boron coordination. The fraction of four-fold coordinated B increases with increasing redox ratio of iron. Increase of Fe^{2+}/Fe^{3+} ratio provides a mechanism for increasing four-fold coordinated boron content. The reason could be twofold. On one hand, Fe^{2+} species were proven to play a modifier role in iron rich glasses. The increase of FeO can increase the modifier content, hence the R value, hence affect the $^{[3]}B/^{[4]}B$ ratio [97,98]. On the other hand, there are two glass formers (SiO_2 and B_2O_3) and two intermediates (Al_2O_3 and Fe_2O_3) coexist in FNAB glasses, causing the multiple roles of the network modifiers. They can play the role of modifier to create non-bridging oxygen or serve as charge compensators to the four-fold coordinated network forming species: $[BO_4]^-$, $[AlO^4]^-$, $[FeO^4]^-$. So there is a competition for modifier cations, either Na^+ or Fe^{2+}. The boron coordination is quite affected by the change in redox ratio of two different types of iron ions. With increasing Fe^{2+}in expanse of Fe^{3+}, i.e. in a more reducing environment, B^{3+}ions are converted from three-fold to four-fold coordination.

Doweidar et al. studied the competition of B^{3+} and Al^{3+} for Na^+ for charge compensation in a series of sodium boroaluminosilciate glasses [99]. They reported that at constant modifier content the increased Al_2O_3 caused decrease of four-coordinated B content and concluded that Na^+ prefers to charge compensate $[AlO_4]^-$ to $[BO_4]^{-}$[99]. Later Wu and Stebbins[97] studied glasses with two modifiers (Na^+ and Ca^{2+}), increase of Al_2O_3 lead to decrease of $^{[4]}B$ in alumino-borosilicates. In addition, in a recent simulation work, Ha and Garofalini[84] reported that the ratio of $^{[3]}B/^{[4]}B$ is affected by the ratio of Al_2O_3/B_2O_3, indicating increased Al_2O_3 resulting in decreased $^{[4]}B$ under a constant concentration of network modifiers. Therefore, the effect of substitution of different glass formers with constant amount of glass former is also worth taking into consideration for future studies.

From simulation point of view, boron coordination can also change as a function of cooling rate and system size. In an earlier study we have investigated the two effects on boron coordination, as well as other structural features and properties, of a sodium borosilicate glass.[102] It was found that when system size is above 1,200 atoms, boron coordination number stabilizes and showed less variations.[102] Boron coordination also increases with slower cooling rate. In this work, we used the 5K/ps cooling rate, the same as the one used for developing the potentials.[59]

The simulation cell sizes of this are around 10,000 atoms for each composition, hence the effects of system size and cooling on various glass compositions are minimal in this work hence they are comparable. Additionally, the theoretical value of the boron coordination (in Fig. 5) was based on the model of sodium and potassium boroaluminosilicate glasses.[103] As boron coordination number is potentially a function of cation field strength as well, hence different type of modifier cation can have different effect, as shown in recent simulation[104] and experimental[12,105] studies. This might partially contribute to the difference between the theory and simulation results shown in Fig. 5. So the composition dependence potentials should ideally consider this effect as well. However, that would also increase complexity of the model.

4.2 Determination of ferric/ferrous equilibria

In alkali and alkaline earth borosilicate glasses, ferric and ferrous species equilibria are controlled by the glass compositions, oxygen partial pressure and temperature profile during the glass processing. In practice, Mössbauer spectroscopy, wet chemistry and optical spectroscopy can be used to determine redox ratio in glass[100]. Studies from Goldman[101] suggested a linear dependence of log (Fe^{3+}/Fe^{2+})with log(pO_2) and 1/T and redox equilibria is not dependent on total iron content in a small range of Fe_2O_3 of 0.9 to 0.5 mole percentage. Hence, the study derived the oxidation-reduction reaction to be written as:

$$Fe^{2+} + (1/4)O_2 + (3/2)O_2^- = FeO_2^- \quad (3)$$

In our simulations, the starting composition (FNAB) contains 100% of Fe_2O_3, which is gradually reduced to 0% Fe_2O_3 and 100% FeO. It is worth noting that in the process, we used $(FeO)_2$ to Fe_2O_3 substitution to maintain constant total iron (Table 2). Therefore, the compositions under study cover a wide range and systematic change of iron redox equilibria. This is to ensure the effect of changing redox ratio on the structure of the aluminum borosilicate glasses in FNAB series. Experimentally, it was found that more ferric (Fe^{3+}) ions was reduced to ferrous (Fe^{2+}) when iron oxide was below 5 mol% in sodium silicate glasses and the highest fraction of Fe^{2+} from Mössbauer spectroscopy was 11%. Less iron reduction was observed with higher amount (> 5 mol%) of iron oxide concentration (the highest amount of iron oxide can be incorporated was found to be 18 mol%).[67]

Our results indicate a competition of the glass intermediate cations, particularly those negatively charged four-fold coordinated units $[MO_4]^-$ (M=Fe, Al, and B), for glass modifier cations such as Na^+ and Fe^{2+} for local charge compensation. For both of the species, from the partial pair distribution function (PDF) in Fig. 10, it is not very clear which glass intermediate cation has the preference to be charge compensated first as the PDF peak shape and intensities are similar. However, the cation preference (Table 9) shows that the preference sequence for Na^+ charge compensation is $Fe^{3+} \geq Al^{3+} > B^{3+}$. While for Fe^{2+}, the charge compensation sequence is $Fe^{3+} > Al^{3+} > B^{3+}$. The difference between Na^+ and Fe^{2+} is that, Fe^{2+} has higher preference to be with Fe^{3+} than Al^{3+} for charge compensation while for Na^+, the preference of the two are similar. Hence the tendency of attracting modifier cations for charge compensation of Al^{3+} and ferric Fe^{3+} are similar, which can be explained by the fact that both of them have similar ionic radii which is reflected from their similar cation-oxygen bond distances (1.77 Å for Al-O and 1.86 Å for Fe^{3+}-O as shown in Fig. 3). Although B^{3+} has even smaller ionic radii as reflected by shorter B-O bond distances (1.4-1.5 Å depending on the composition), there is probably higher covalency in the B-O bond than the Al-O and Fe^{3+}-O bonds, hence B^{3+} has lower capability to attract the modifier cations and its preference for charge compensation follows that of Al^{3+} and Fe^{3+}, which is supported from our simulation results.

Furthermore, modifier cations can play dual roles of charge compensation and creation of non-bridging oxygen in aluminosilicate and boroaluminosilicate glasses.[12,104,105] The exact role they play depends on the type of modifier cations and the glass composition. It has been known that alkali cations such as Na^+ is more effective for charge compensation of charged groups $[MO_4]^-$ hence then while higher charged modifier cations such as Mg^{2+} and Ca^{2+} are less effective in charge compensation and they favor more of non-bridging oxygen formation.[12,104,105] It is expected Fe^{2+} would play similar role as the alkali earth cations. Hence for alkali cations, they play the charge compensation role first then the remaining ones create non-bridging oxygen while for the higher charged modifier cations the sequence is opposite. The information of these subtle structural details would enhance our understanding of glass chemistry so we can better design glass composition with desired structures and properties.

5 Conclusions

The structures of $53.32SiO_2$-$9.12B_2O_3$-$23.93Na_2O$-$6.40Al_2O_3$-$(7.22-x)Fe_2O_3$-$2xFeO$ (x=0 to 7.22) have been investigated by using MD simulations with recently developed partial charge pairwise boron potentials and compatible parameters for ferrous and ferric iron species. Total correlation functions, coordination distributions, and bond angle distributions were used to characterize the iron-containing boroaluminosilicate glasses structures with various redox ratios. It was found that an increase in the Fe^{2+} concentration decreases the fraction of three-fold coordinated boron and increases the concentration of four-fold coordinated boron. Fe^{3+} ions have a Fe-O bond distance of 1.86 Å and an average coordination number of 4, hence plays the role of a glass former in these glasses. Fe^{2+}, on the other hand, has a Fe-O bond distance of 2.07 Å and an average coordination number of 4.6 hence play the role of a modifier. This is further supported from the shape of Fe-O pair distribution function and bond O-Fe-O bond angle distribution. The structural role of Na^+ and Fe^{2+} as a charge compensator and their preference for charge compensation of negatively charged $[MO_4]^-$ ($M=B^{3+}$, Al^{3+} and Fe^{3+}) units were also investigated based on the simulation results. The preferential sequence for Na^+ of charge compensation is $Fe^{3+} \geq Al^{3+} > B^{3+}$ while that for Fe^{2+} is $Fe^{3+} > Al^{3+} > B^{3+}$. For Fe^{2+}, it can also favor the role of non-bridging oxygen creation. Hence further experimental and simulation work is needed to clarify the exact structural of Fe^{2+} as compared to other modifiers. This study thus sheds light on the structural role of iron oxide on the structures of silicate and borosilicate glasses that are important in glass technologies and geosciences. It also provides insights on the important interplay of mixing various glass formers and charge compensations in aluminoborosilicate glass as a function of iron redox ratio. The results also show classical MD simulations with well-developed parameters can be used to understand the transition metals with multi oxidation states in silicate glasses.

Acknowledgements

This work was supported by the Center for Performance and Design of Nuclear Waste Forms and Containers, an Energy Frontier Research Center funded by the U.S. Department of Energy, Office of Science, Basic Energy Sciences (BES) under Award # DE-SC0016584 and U.S. National Science Foundation (project #16622288).

References

(1) Fortino, M.; Berselli, A.; Stone-Weiss, N.; Deng, L.; Goel, A.; Du, J.; Pedone, A. Assessment of Interatomic Parameters for the Reproduction of Borosilicate Glass Structures via DFT-GIPAW Calculations. *J. Am. Ceram. Soc.* **2019**, No. June, 7225–7243.

(2) Smedskjaer, M. M.; Mauro, J. C.; Youngman, R. E.; Hogue, C. L.; Potuzak, M.; Yue, Y. Topological Principles of Borosilicate Glass Chemistry. *J. Phys. Chem. B* **2011**, *115*, 12930–12946.

(3) Phillips, J. C.; Kerner, R. Structure and Function of Window Glass and Pyrex. *J. Chem. Phys.* **2008**, *128*.

(4) Weber, W. J.; Ewing, R. C.; Angell, C. A.; Arnold, G. W.; Delaye, J. M.; Hobbs, L. W.; Price, D. L. Waste and Plutonium Disposition. *J. Mater. Res.* **1997**, *12*, 1946–1978.

(5) Gin, S.; Abdelouas, A.; Criscenti, L. J.; Ebert, W. L.; Ferrand, K.; Geisler, T.; Harrison, M. T.; Inagaki, Y.; Mitsui, S.; Mueller, K. T.; et al. An International Initiative on Long-Term Behavior of High-Level Nuclear Waste Glass. *Mater. Today* **2013**, *16*, 243–248.

(6) Yue, Y.; Tuheen, M. I.; Du, J. Borosilicate Glasses. In *EncyclopediaofMaterials:TechnicalCeramicsandGlasses*; Elsevier, 2021; pp 1–21.

(7) Du, J.; Montorsi, M.; Barbi, S.; Lu, X. Rare Earth and Transition Metal Containing Glasses. In *Atomistic Simulations of Glasses Fundamentals and Applications*; Wiley, 2022; pp 367–438.

(8) Lu, X.; Deng, L.; Huntley, C.; Ren, M.; Kuo, P. H.; Thomas, T.; Chen, J.; Du, J. Mixed Network Former Effect on Structure, Physical Properties, and Bioactivity of 45S5 Bioactive Glasses: An Integrated Experimental and Molecular Dynamics Simulation Study. *J. Phys. Chem. B* **2018**, *122*, 2564–2577.

(9) Fábián, M.; Sváb, E.; Proffen, T.; Veress, E. Structure Study of Multi-Component Borosilicate Glasses from High-Q Neutron Diffraction Measurement and RMC Modeling. *J. Non. Cryst. Solids* **2008**, *354*, 3299–3307.

(10) Dell, W. J.; Bray, P. J.; Xiao, S. Z. 11B NMR Studies and Structural Modeling of Na2OB2O3SiO2 Glasses of High Soda Content. *J. Non. Cryst. Solids* **1983**, *58*, 1–16.

(11) Bouty, O.; Delaye, J. M.; Peuget, S. Europium Structural Effect on a Borosilicate Glass of Nuclear Interest. *Procedia Chem.* **2012**, *7*, 540–547.

(12) Wu, J.; Stebbins, J. F.; Rouxel, T. Cation Field Strength Effects on Boron Coordination in Binary Borate Glasses. *J. Am. Ceram. Soc.* **2014**, *97*, 2794–2801.

(13) Dell, W. J.; Bray, P. J.; Xiao, S. Z. ^{11}B NMR Studies and Structural Modeling of $NaO-B_2O_3-SiO_2$ Glasses of High Soda Content. *J. Non. Cryst. Solids* **1983**, *58*, 1–16.

(14) Lu, X.; Deng, L.; Du, J.; Vienna, J. D. Predicting Boron Coordination in Multicomponent Borate and Borosilicate Glasses Using Analytical Models and Machine Learning. *J. Non. Cryst. Solids* **2021**, *553*, 120490.

(15) Bisbrouck, N.; Bertani, M.; Angeli, F.; Charpentier, T.; de Ligny, D.; Delaye, J. M.; Gin, S.; Micoulaut, M. Impact of Magnesium on the Structure of Aluminoborosilicate Glasses: A Solid-State NMR and Raman Spectroscopy Study. *J. Am. Ceram. Soc.* **2021**, *104*, 4518–4536.

(16) Du, L. S.; Stebbins, J. F. Network Connectivity in Aluminoborosilicate Glasses: A High-Resolution 11B, 27Al and 17O NMR Study. *J. Non. Cryst. Solids* **2005**, *351*, 3508–3520.

(17) Youngman, R. NMR Spectroscopy in Glass Science: A Review of the Elements. *Materials (Basel).* **2018**, *11*.

(18) Waychunas, G. A.; Brown, G. E.; Ponader, C. W.; Jackson, W. E. Evidence from X-Ray Absorption for Network-Forming Fe2+ in Molten Alkali Silicates. *Nature* **1988**, *332*, 251–253.

(19) Di Genova, D.; Hess, K. U.; Chevrel, M. O.; Dingwell, D. B. Models for the Estimation of Fe3+/Fetot Ratio in Terrestrial and Extraterrestrial Alkali- and Iron-Rich Silicate Glasses Using Raman Spectroscopy. *Am. Mineral.* **2016**, *101*, 943–952.

(20) Le Losq, C.; Cicconi, M. R.; Neuville, D. R. Iron in Silicate Glasses and Melts: Implications for Volcanological Processes. *ESSOAr* **2020**, 1–29.

(21) Waseda, Y.; Toguri, J. M. The Structure of the Molten FeO-SiO2 System. *Metall. Trans. B* **1978**, *9*, 595–601.

(22) Di Genova, D.; Zandona, A.; Deubener, J. Unravelling the Effect of Nano-Heterogeneity on the Viscosity of Silicate Melts: Implications for Glass Manufacturing and Volcanic Eruptions. *J. Non. Cryst. Solids* **2020**, *545*, 120248.

(23) Yue, Y.; Korsgaard, M.; Kirkegaard, L. F.; Heide, G. Formation of a Nanocrystalline Layer on the Surface of Stone Wool Fibers. *J. Am. Ceram. Soc.* **2009**, *92*, 62–67.

(24) Drewitt, J. W. E.; Sanloup, C.; Bytchkov, A.; Brassamin, S.; Hennet, L. Structure of (FexCa1-XO)y(SiO 2)1-y Liquids and Glasses from High-Energy x-Ray Diffraction: Implications for the Structure of Natural Basaltic Magmas. *Phys. Rev. B - Condens. Matter Mater. Phys.* **2013**, *87*.

(25) Alderman, O. L. G.; Benmore, C. J.; Weber, J. K. R.; Skinner, L. B.; Tamalonis, A. J.; Sendelbach, S.; Hebden, A.; Williamson, M. A. The Structure of Liquid UO2−x in Reducing Gas Atmospheres. *Appl. Phys. Lett.* **2017**, *110*, 1–6.

(26) Ahmadzadeh, M.; Scrimshire, A.; Mottram, L.; Stennett, M. C.; Neil, C.; Bingham, P. A.; Mccloy, J. S. Revision 1 (Correction Date 9 Feb 2020). **2020**.

(27) Nienhuis, E. T.; Tuheen, M.; Du, J.; McCloy, J. S. In Situ Pair Distribution Function Analysis of Crystallizing Fe-Silicate Melts. *J. Mater. Sci.* **2021**, *56*, 5637–5657.

(28) Mysen, B. O. The Structural Behavior of Ferric and Ferrous Iron in Aluminosilicate Glass near Meta-Aluminosilicate Joins. *Geochim. Cosmochim. Acta* **2006**, *70*, 2337–2353.

(29) Wang, Z.; Cooney, T. F.; Sharma, S. K. In Situ Structural Investigation of Iron-Containing Silicate Liquids and Glasses. *Geochim. Cosmochim. Acta* **1995**, *59*, 1571–1577.

(30) Weigel, C.; Cormier, L.; Calas, G.; Galoisy, L.; T. Bowron, D. Nature and Distribution of Iron Sites in a Sodium Silicate Glass Investigated by Neutron Diffraction and EPSR Simulation. *J. Non. Cryst. Solids* **2008**, *354*, 5378–5385.

(31) Cochain, B.; Neuville, D. R.; Henderson, G. S.; McCammon, C. A.; Pinet, O.; Richet, P. Effects of the Iron Content and Redox State on the Structure of Sodium Borosilicate Glasses: A Raman, Mössbauer and Boron k-Edge Xanes Spectroscopy Study. *J. Am. Ceram. Soc.* **2012**, *95*, 962–971.

(32) Virgo, D.; Mysen, B. O. The Structural State of Iron in Oxidized vs. Reduced Glasses at 1 Atm: A57Fe Mössbauer Study. *Phys. Chem. Miner.* **1985**, *12*, 65–76.

(33) Cochain, B.; Neuville, D. R.; Henderson, G. S.; McCammon, C. A.; Pinet, O.; Richet, P. Effects of the Iron Content and Redox State on the Structure of Sodium Borosilicate Glasses: A Raman, Mössbauer and Boron K-Edge XANES Spectroscopy Study. *J. Am. Ceram. Soc.* **2012**, *95*, 962–971.

(34) Sun, W.; Du, J. Interfacial Structures of Spinel Crystals with Borosilicate Nuclear Waste Glasses from Molecular Dynamics Simulations. *J. Am. Ceram. Soc. 0*.

(35) Collin, M.; Fournier, M.; Frugier, P.; Charpentier, T.; Moskura, M.; Deng, L.; Ren, M.; Du, J.; Gin, S. Structure of International Simple Glass and Properties of Passivating Layer Formed in Circumneutral PH Conditions. *npj Mater. Degrad.* **2018**, *2*, 4.

(36) Rushton, M. J. D.; Grimes, R. W.; Owens, S. L. Partial Ordering of Glass Networks Adjacent to Simulated Glass–Crystal Interfaces. *J. Non. Cryst. Solids* **2011**, *357*, 3278–3287.

(37) Ojovan, M. I.; Lee, W. E. Chapter 17 - Immobilisation of Radioactive Wastes in Glass. In *An Introduction to Nuclear Waste Immobilisation*; Ojovan, M. I., Lee, W. E., Eds.; Elsevier: Oxford, 2005; pp 213–249.

(38) Donnay, G.; Schairer, J. F.; Donnay, J. D. H. Nepheline Solid Solutions. *Mineral. Mag. J. Mineral. Soc.* **1959**, *32*, 93–109.

(39) Deshkar, A.; Ahmadzadeh, M.; Scrimshire, A.; Han, E.; Bingham, P. A.; Guillen, D.; McCloy, J.; Goel, A. Crystallization Behavior of Iron- and Boron-Containing Nepheline (Na2O·Al2O3·2SiO2) Based Model High-Level Nuclear Waste Glasses. *J. Am. Ceram. Soc.* **2019**, *102*, 1101–1121.

(40) Mysen, B. O. Relationships between Silicate Melt Structure and Petrologic Processes. *Earth-Science Rev.* **1990**, *27*, 281–365.

(41) Smedskjaer, M. M.; Mauro, J. C.; Sen, S.; Deubener, J.; Yue, Y. Impact of Network Topology on Cationic Diffusion and Hardness of Borate Glass Surfaces. *J. Chem. Phys.* **2010**, *133*.

(42) Oxidation State and Coordination of Fe in Minerals: An Fe K-XANES Spectroscopic Study . *American Mineralogist* . 2001, p 714.

(43) Volovetskii, M. V; Lukanin, O. A.; Rusakov, V. S.; Kargal'tsev, A. A. Influence of Oxygen Fugacity and Temperature on the Redox State of Iron in Natural Silicic Aluminosilicate Melts. *Geochemistry Int.* **2012**, *50*, 330–343.

(44) Henderson, G.; De Groot, F.; Moulton, B. X-Ray Absorption Near-Edge Structure (XANES) Spectroscopy. *Rev. Mineral. Geochemistry* **2014**, *78*, 75–138.

(45) Hannoyer, B.; Lenglet, M.; Dürr, J.; Cortes, R. Spectroscopic Evidence of Octahedral Iron (III) in Soda-Lime Silicate Glasses. *J. Non. Cryst. Solids* **1992**, *151*, 209–216.

(46) Glazkova, Y. S.; Kalmykov, S. N.; Presnyakov, I. A.; Stefanovskaya, O. I.; Stefanovsky, S. V. The Structural State of Iron in Multicomponent Aluminum Iron Borosilicate Glass Depending on Their Composition and Synthesis Conditions. *Glas. Phys. Chem.* **2015**, *41*, 367–377.

(47) Magnien, V.; Neuville, D. R.; Cormier, L.; Mysen, B. O.; Briois, V.; Belin, S.; Pinet, O.; Richet, P. Kinetics of Iron Oxidation in Silicate Melts: A Preliminary XANES Study. *Chem. Geol.* **2004**,

213, 253–263.

(48) Burns, R. G. Mineral Mössbauer Spectroscopy: Correlations between Chemical Shift and Quadrupole Splitting Parameters. *Hyperfine Interact.* **1994**, *91*, 739–745.

(49) Weigel, C.; Mccammon, C.; Keppler, H. High-Temperature Mossbauer Spectroscopy: A Probe for the Relaxation Time of Fe Species in Silicate Melts and Glasses. *Am. Mineral.* **2010**, *95*, 1701–1707.

(50) Jackson, W. E.; Farges, F.; Yeager, M.; Mabrouk, P. A.; Rossano, S.; Waychunas, G. A.; Solomon, E. I.; Brown, G. E. Multi-Spectroscopic Study of Fe(II) in Silicate Glasses: Implications for the Coordination Environment of Fe(II) in Silicate Melts. *Geochim. Cosmochim. Acta* **2005**, *69*, 4315–4332.

(51) Delaye, J. M. Modeling of Multicomponent Glasses: A Review. *Curr. Opin. Solid State Mater. Sci.* **2001**, *5*, 451–454.

(52) Kieu, L. H.; Delaye, J. M.; Cormier, L.; Stolz, C. Development of Empirical Potentials for Sodium Borosilicate Glass Systems. *J. Non. Cryst. Solids* **2011**, *357*, 3313–3321.

(53) Cormier, L.; Galoisy, L.; Delaye, J.-M.; Ghaleb, D.; Calas, G. Short- and Medium-Range Structural Order around Cations in Glasses: A Multidisciplinary Approach. *Comptes Rendus l'Académie des Sci. - Ser. IV - Physics-Astrophysics* **2001**, *2*, 249–262.

(54) Barlet, M.; Kerrache, A.; Delaye, J.-M.; Rountree, C. L. SiO2–Na2O–B2O3 Density: A Comparison of Experiments, Simulations, and Theory. *J. Non. Cryst. Solids* **2013**, *382*, 32–44.

(55) Deng, L.; Du, J. Development of Effective Empirical Potentials for Molecular Dynamics Simulations of the Structures and Properties of Boroaluminosilicate Glasses. *J. Non. Cryst. Solids* **2016**, *453*, 177–194.

(56) Todorov, I.; Smith, W.; Cheshire, U. The DL POLY 4 User Manual. *STFC, STFC Daresbury …* **2011**, No. January.

(57) Pedone, A. Properties Calculations of Silica-Based Glasses by Atomistic Simulations Techniques : A Review. **2009**, 20773–20784.

(58) Du, J.; Cormack, A. N. Molecular Dynamics Simulation of the Structure and Hydroxylation of Silica Glass Surfaces. *J. Am. Ceram. Soc.* **2005**, *88*, 2532–2539.

(59) Deng, L.; Du, J. Development of Boron Oxide Potentials for Computer Simulations of Multicomponent Oxide Glasses. *J. Am. Ceram. Soc.* **2019**, *102*, 2482–2505.

(60) Cornell, R.M.; Schwertmann, U. Crystal Structure. In *The Iron Oxides: Structure, Properties, Reactions, Occurences and Uses. second edition.*; WILEY-VCH Verlag, 2003; pp 9–38.

(61) Liao, P.; Carter, E. A. Ab Initio DFT + U Predictions of Tensile Properties of Iron Oxides. *J. Mater. Chem.* **2010**, *20*, 6703–6719.

(62) Du, J.; Cormack, A. N. Erratum: "The Medium Range Structure of Sodium Silicate Glasses: A Molecular Dynamics Simulation" by J. Du and A.N. Cormack (Journal of Non-Crystalline Solids (2004) 349 (66-79) DOI:10.1016/j.Jnoncrysol.2004.08.264). *J. Non. Cryst. Solids* **2005**, *351*, 956.

(63) Zirl, D. M.; Garofalini, S. H. Structure of Sodium Aluminosilicate Glasses. *J. Am. Ceram. Soc.*

1990, *73*, 2848–2856.

(64) Greaves, G. N.; Fontaine, A.; Lagarde, P.; Raouxt, D.; Gorman, S. J. Local Structure of Silicate Glasses. *Nature* **1981**, *293*, 611–616.

(65) Xiang, Y.; Du, J.; Smedskjaer, M. M.; Mauro, J. C. Structure and Properties of Sodium Aluminosilicate Glasses from Molecular Dynamics Simulations. *J. Chem. Phys.* **2013**, *139*.

(66) McKeown, D. A.; Waychunas, G. A.; Brown, G. E. Exafs and Xanes Study of the Local Coordination Environment of Sodium in a Series of Silica-Rich Glasses and Selected Minerals within the Na2OAl2O3SiO2 System. *J. Non. Cryst. Solids* **1985**, *74*, 325–348.

(67) Holland, D.; Mekki, A.; Gee, I. A.; McConville, C. F.; Johnson, J. A.; Johnson, C. E.; Appleyard, P.; Thomas, M. Structure of Sodium Iron Silicate Glass - a Multi-Technique Approach. *J. Non. Cryst. Solids* **1999**, *253*, 192–202.

(68) Majérus, O.; Cormier, L.; Calas, G.; Beuneu, B. Temperature-Induced Boron Coordination Change in Alkali Borate Glasses and Melts. *Phys. Rev. B - Condens. Matter Mater. Phys.* **2003**, *67*, 1–7.

(69) Mozzi, R. L.; Warren, B. E. The Structure of Vitreous Boron Oxide. *J. Appl. Crystallogr.* **1970**, *3*, 251–257.

(70) Pedesseau, L.; Ispas, S.; Kob, W. First-Principles Study of a Sodium Borosilicate Glass-Former. I. the Liquid State. *Phys. Rev. B - Condens. Matter Mater. Phys.* **2015**, *91*, 1–14.

(71) Magini, M.; Sedda, A. F.; Licheri, G.; Paschina, G.; Piccaluga, G.; Pinna, G.; Cocco, G. On the Coordination of Iron Ions in Sodium Borosilicate Glasses. *J. Non. Cryst. Solids* **1984**, *65*, 145–159.

(72) Lu, X.; Ren, M.; Deng, L.; Benmore, C. J.; Du, J. Structural Features of ISG Borosilicate Nuclear Waste Glasses Revealed from High-Energy X-Ray Diffraction and Molecular Dynamics Simulations. *J. Nucl. Mater.* **2019**, *515*, 284–293.

(73) Ren, M.; Du, J. Structural Origin of the Thermal and Diffusion Behaviors of Lithium Aluminosilicate Crystal Polymorphs and Glasses. *J. Am. Ceram. Soc.* **2016**, *99*, 2823–2833.

(74) Farges, F.; Lefrère, Y.; Rossano, S.; Berthereau, A.; Calas, G.; Brown, G. E. The Effect of Redox State on the Local Structural Environment of Iron in Silicate Glasses: A Combined XAFS Spectroscopy, Molecular Dynamics, and Bond Valence Study. *J. Non. Cryst. Solids* **2004**, *344*, 176–188.

(75) Mysen, B. O.; Virgo, D. Structure and Properties of Silicate Glasses and Melts; Theories and Experiment BT - Advanced Mineralogy: Volume 1 Composition, Structure, and Properties of Mineral Matter: Concepts, Results, and Problems; Marfunin, A. S., Ed.; Springer Berlin Heidelberg: Berlin, Heidelberg, 1994; pp 238–254.

(76) Booz, J.; Braby, L.; Coyne, J.; Kliauga, P.; Lindborg, L.; Menzel, H.-G.; Parmentier, N. 1. Introduction. *Reports Int. Comm. Radiat. Units Meas.* **1983**, *os-19*, 1–3.

(77) Wang, M.; You, J.; Sobol, A.; Lu, L.; Wang, J.; Xie, Y. In-Situ Studies of Structure Transformation and Al Coordination of $KAl(MoO_4)_2$ during Heating by High Temperature Raman and (27)Al NMR Spectroscopies. *Mater. (Basel, Switzerland)* **2017**, *10*, 310.

(78) Thompson, L. M.; Stebbins, J. F. Non-Stoichiometric Non-Bridging Oxygens and Five-Coordinated Aluminum in Alkaline Earth Aluminosilicate Glasses: Effect of Modifier Cation Size. *J. Non. Cryst. Solids* **2012**, *358*, 1783–1789.

(79) Yiannopoulos, Y. D.; Chryssikos, G. D.; Kamitsos, E. I. Structure and Properties of Alkaline Earth Borate Glasses. *Phys. Chem. Glas.* **2001**, *42*, 164–172.

(80) Wright, A. C.; Dalba, G.; Rocca, F.; Vedishcheva, N. M. Borate versus Silicate Glasses: Why Are They so Different? *Phys. Chem. Glas. Eur. J. Glas. Sci. Technol. Part B* **2010**, *51*, 233–265.

(81) Ghoneim, N. A.; Abbas, A. F. Thermal Expansion of High Lead Borate Glasses and the Boric Oxide Anomaly. *Thermochim. Acta* **1983**, *66*, 91–103.

(82) Yun, Y. H.; Bray, P. J. Nuclear Magnetic Resonance Studies of the Glasses in the System K2OB2O3P2O5. *J. Non. Cryst. Solids* **1978**, *30*, 45–60.

(83) Yun, Y.H.; Feller, S.A.; Bray, P. J. Correction on Addendim to "Nuclear Magnetic Resonance Studies of the Glasses in the System Na2O-B2O3-SiO2." *J. Non* **1979**, *33*, 273–277.

(84) Ha, M. T.; Garofalini, S. H. Local Structure of Network Modifier to Network Former Ions in Soda-Lime Alumino-Borosilicate Glasses. *J. Am. Ceram. Soc.* **2017**, *100*, 563–573.

(85) Xiang, Y.; Du, J. Effect of Strontium Substitution on the Structure of 45S5 Bioglasses. *Chem. Mater.* **2011**, *23*, 2703–2717.

(86) Rimsza, J. M.; Du, J. Structural and Mechanical Properties of Nanoporous Silica. *J. Am. Ceram. Soc.* **2014**, *97*, 772–781.

(87) Du, J.; Cormack, A. N. The Medium Range Structure of Sodium Silicate Glasses: A Molecular Dynamics Simulation. *J. Non. Cryst. Solids* **2004**, *349*, 66–79.

(88) Poulsen, H. F.; Neuefeind, J.; Neumann, H. B.; Schneider, J. R.; Zeidler, M. D. Amorphous Silica Studied by High Energy X-Ray Diffraction. *J. Non. Cryst. Solids* **1995**, *188*, 63–74.

(89) Grimley, D. I.; Wright, A. C.; Sinclair, R. N. Neutron Scattering from Vitreous Silica IV. Time-of-Flight Diffraction. *J. Non. Cryst. Solids* **1990**, *119*, 49–64.

(90) Sun, W.; Du, J. Local Ordering and Interfacial Structure between Spinel Crystal and Aluminosilicate Glasses from Molecular Dynamics Simulations. *Int. J. Appl. Glas. Sci.* **2018**, No. May.

(91) Loewenstein, W. The Distribution of Aluminum in the Tetrahedra of Silicates and Aluminates. *Am. Mineral.* **1954**, *39*, 92–96.

(92) Stebbins, J. Aluminium Avoidance Avoided. *Nature* **1987**, *330*, 13–14.

(93) Dongol, R.; Wang, L.; Cormack, A. N.; Sundaram, S. K. Molecular Dynamics Simulation of Sodium Aluminosilicate Glass Structures and Glass Surface-Water Reactions Using the Reactive Force Field (ReaxFF). *Appl. Surf. Sci.* **2018**, *439*, 1103–1110.

(94) Bechgaard, T. K.; Scannell, G.; Huang, L.; Youngman, R. E.; Mauro, J. C.; Smedskjaer, M. M. Structure of MgO/CaO Sodium Aluminosilicate Glasses: Raman Spectroscopy Study. *J. Non. Cryst. Solids* **2017**, *470*, 145–151.

(95) Tilocca, A.; Cormack, A. N.; De Leeuw, N. H. The Structure of Bioactive Silicate Glasses: New Insight from Molecular Dynamics Simulations. *Chem. Mater.* **2007**, *19*, 95–103.

(96) Zhang, P.; Dunlap, C.; Florian, P.; Grandinetti, P. J.; Farnan, I.; Stebbins, J. F. Silicon Site Distributions in an Alkali Silicate Glass Derived by Two-Dimensional 29Si Nuclear Magnetic Resonance. *J. Non. Cryst. Solids* **1996**, *204*, 294–300.

(97) Wu, J.; Stebbins, J. F. Effects of Cation Field Strength on the Structure of Aluminoborosilicate Glasses: High-Resolution 11B, 27Al and 23Na MAS NMR. *J. Non. Cryst. Solids* **2009**, *355*, 556–562.

(98) Smedskjaer, M. M.; Youngman, R. E.; Mauro, J. C. Principles of Pyrex ◆ Glass Chemistry: Structure◆property Relationships. *Appl. Phys. A* **2014**, *116*, 491–504.

(99) Doweidar, H.; Moustafa, Y.; Abdel-maksoud, S.; SILIM, H. Properties of Na2O–Al2O3–B2O3 Glasses. *Mater. Sci. Eng. A-structural Mater. Prop. Microstruct. Process. - MATER SCI ENG A-STRUCT MATER* **2001**, *301*, 207–212.

(100) Bingham, P. A.; Parker, J. M.; Searle, T.; Williams, J. M.; Fyles, K. Redox and Clustering of Iron in Silicate Glasses. *J. Non. Cryst. Solids* **1999**, *253*, 203–209.

(101) GOLDMAN, D. S. Oxidation Equilibrium of Iron in Borosilicate Glass. *J. Am. Ceram. Soc.* **1983**, *66*, 205–209.

(102) Deng, L.; Du, J. Effects of System Size and Cooling Rate on the Structure and Properties of Sodium Borosilicate Glasses from Molecular Dynamics Simulations. *J. Chem. Phys.* **2018**, *148*, 024504.

(103) Du, L.; Stebbins, J. F. Network Connectivity in Aluminoborosilicate Glasses : **2005**, *351*, 3508–3520.

(104) Tuheen, M. I.; Du, J. Effect of Modifier Cation Field Strength on the Structures of Magnesium Oxide Containing Aluminoborosilicate Glasse. *Int. J. Appl. Glas. Sci.* **2022** (accepted for publication).

(105) Bisbrouck, N.; Bertani, M.; Angeli, F.; Charpentier, T.; de Ligny, D.; Delaye, J. M.; Gin, S.; Micoulaut, M. Impact of Magnesium on the Structure of Aluminoborosilicate Glasses: A Solid-State NMR and Raman Spectroscopy Study. *J. Am. Ceram. Soc.* **2021**, *104*, 4518–4536.